Geochemistry, Geophysics, Geosystems

RESEARCH ARTICLE
10.1029/2018GC007941

A Mantle Plume Origin for the Scandinavian Dyke Complex: A "Piercing Point" for 615 Ma Plate Reconstruction of Baltica?

Christian Tegner[1], Torgeir B. Andersen[2], Hans Jørgen Kjøll[2], Eric L. Brown[1], Graham Hagen-Peter[1], Fernando Corfu[2], Sverre Planke[2], and Trond H. Torsvik[2,3]

[1]Centre of Earth System Petrology, Department of Geoscience, Aarhus University, Aarhus, Denmark, [2]Centre for Earth Evolution and Dynamics, University of Oslo, Oslo, Norway, [3]School of Geosciences, University of Witwatersrand, Johannesburg, South Africa

Abstract The origin of Large Igneous Provinces (LIPs) associated with continental breakup and the reconstruction of continents older than ca. 320 million years (pre-Pangea) are contentious research problems. Here we study the petrology of a 615–590 Ma dolerite dyke complex that intruded rift basins of the magma-rich margin of Baltica and now is exposed in the Scandinavian Caledonides. These dykes are part of the Central Iapetus Magmatic Province (CIMP), a LIP emplaced in Baltica and Laurentia during opening of the Caledonian Wilson Cycle. The >1,000-km-long dyke complex displays lateral geochemical zonation from enriched to depleted basaltic compositions from south to north. Geochemical modelling of major and trace elements shows these compositions are best explained by melting hot mantle 75–250 °C above ambient mantle. Although the trace element modelling solutions are nonunique, the best explanation involves melting a laterally zoned mantle plume with enriched and depleted peridotite lithologies, similar to present-day Iceland and to the North Atlantic Igneous Province. The origin of CIMP appears to have involved several mantle plumes. This is best explained if rifting and breakup magmatism coincided with plume generation zones at the margins of a Large Low Shear-wave Velocity Province (LLSVP) at the core mantle boundary. If the LLSVPs are quasi-stationary back in time as suggested in recent geodynamic models, the CIMP provides a guide for reconstructing the paleogeography of Baltica and Laurentia 615 million years ago to the LLSVP now positioned under the Pacific Ocean. Our results provide a stimulus for using LIPs as piercing points for plate reconstructions.

Key Points:
- The Scandinavian Dyke Complex shows lateral geochemical zoning similar to Iceland today and originated from a hot, zoned mantle plume
- Large igneous provinces generated from mantle plumes can be used as piercing points for plate reconstructions
- 615 million years ago Baltica was located vertically above the edge of a Large Low Shear-wave Velocity Province at the core-mantle boundary

Supporting Information:
- Supporting Information S1
- Data Set S1
- Movie S1

Correspondence to:
C. Tegner,
christian.tegner@geo.au.dk

Citation:
Tegner, C., Andersen, T. B., Kjøll, H. J., Brown, E. L., Hagen-Peter, G., Corfu, F., et al. (2019). A mantle plume origin for the Scandinavian Dyke Complex: A "piercing point" for 615 Ma plate reconstruction of Baltica? *Geochemistry, Geophysics, Geosystems*, *20*. https://doi.org/10.1029/2018GC007941

Received 4 SEP 2018
Accepted 12 JAN 2019
Accepted article online 20 JAN 2019

1. Introduction

The opening and closure of ocean basins is known as the plate tectonic Wilson Cycle (Dewey & Burke, 1974) and was first suggested to explain the North-Atlantic Appalachian-Caledonian mountain belt (Wilson, 1966). Here the first known opening took place 615 to 590 million years ago and led to the inception of the Iapetus Ocean and was associated with the Central Iapetus Magmatic Province (CIMP), a large igneous province (LIP) exposed today as giant dyke complexes and other intrusive complexes and volcanics in north-east America and northwest Europe (Ernst & Bell, 2010). The second opening took place ca. 54 million years ago and led to the inception of the North Atlantic Ocean in the Norwegian-Greenland Sea. Again, the opening was associated with the emplacement of a LIP known as the North Atlantic Igneous Province (NAIP) exposed today in the borderlands of the North-Atlantic and the Norwegian-Greenland Seas (Horni et al., 2017). Volcanic activity within the NAIP commenced at around 62 Ma, more than 300 million years after initiation of post-Caledonian rifting and basin formation but shortly (ca. 8 Myrs) before continental breakup (Torsvik et al., 2014). Following Morgan (1971), Hill (1991), Campbell (2007), and others, Buiter and Torsvik (2014) therefore argued that rifting was initiated and sustained by tectonic forces, but upwelling of mantle plume material (Iceland plume) into the rifted and thinned lithosphere was the trigger for LIP volcanism, final continental breakup, and the beginning of the new Wilson Cycle.

A deep, lower mantle plume origin for present-day Iceland volcanism is supported by seismic tomography (e.g., French & Romanowicz, 2015) and from geochemistry (e.g., Moreira et al., 2001). This has been linked to the plume generation zone (PGZ) at the edge of a Large Low Shear-wave Velocity Province (LLSVP) at the core-mantle boundary (Torsvik et al., 2006). Asserting the origin of the older NAIP and CIMP is more challenging. For NAIP, however, anomalously thick oceanic crust of the Greenland-Iceland-Faroes ridge

(Holbrook et al., 2001) and geochemical enrichment (e.g., Brown & Lesher, 2014; Fitton et al., 1997) point to a mantle plume origin. Moreover, Torsvik et al. (2006) showed that NAIP coincided with a mantle PGZ at around 62 Ma. For CIMP, the records of magmatic crustal thickness and potential mantle plume tracks have been obliterated by the Caledonian Wilson Cycle, and inference about its origin therefore must rely on geology and geochemistry of the magmatic complexes (Andréasson et al., 1998; Hollocher et al., 2007; Puffer, 2002; Seymour & Kumarapeli, 1995).

To further constrain the origin, plate tectonic setting, and deep mantle dynamics of CIMP, we (i) present new geochemical bulk rock data, and Sr isotope data for plagioclase, for the Scandinavian Dyke Complex (also referred to as the "Baltoscandian Dyke Complex"). The dyke swarms are exposed in Caledonian nappes interpreted to have constituted the distal pre-Caledonian continental margin of Baltica (Ottfjället, Sarek, Kebnekaise, Tornetrask, Indre Troms, and Corrovarre); (ii) compiled published compositional data and examined geochemical variations along the more than 1,000-km length of the Scandinavian Dyke Complex; and (iii) modeled mantle melting dynamics. We also compare the geochemistry of CIMP, NAIP, and Iceland and discuss the origin of LIPs associated with the opening phases of the Wilson Cycle. Finally, we produce a new 615 Ma plate reconstruction of Baltica and Laurentia and discuss the potential usage of LIPs as piercing points for plate reconstructions.

2. The CIMP: Chronology and Background

The Central Iapetus Magmatic Province (CIMP) was emplaced over a huge area (>9 million square kilometers; Figure 1) and encompasses magmatic rocks exposed today in NW Europe, Greenland, and NE America that originally formed in the borderlands of the Iapetus Ocean (Ernst & Bell, 2010). Carbonatites and kimberlites were also emplaced throughout the CIMP (615–550 Ma) and have been identified across most of the area covered by CIMP (Ernst & Bell, 2010; Torsvik et al., 2010; Figure 1). Here we focus on the main basaltic events. In Laurentia, the oldest CIMP magmatism (group 1) includes the Long Range (615 ± 2 Ma; Kamo et al., 1989), the >700 km long Grenville (590 ± 2 Ma; Kamo et al., 1995), and the Adirondack dyke swarms (Figure 1). They have compositions similar to continental flood basalts (Puffer, 2002). The Grenville and Adirondack dyke swarms have been interpreted as failed arms of a triple junction centered on the Sutton mountains (Figure 1) and associated with rifting above a CIMP mantle plume (Burke & Dewey, 1973; Hodych & Cox, 2007; Seymour & Kumarapeli, 1995). Younger magmatism (group 2; 565–550 Ma) is also dominated by basaltic dyke swarms that are most intense in the Sutton mountains but also includes mafic and granite plutons and lavas (Cawood et al., 2001; Chew & Van Staal, 2014; Hodych & Cox, 2007). The Sutton mountain dykes have affinities to ocean island basalt (OIB) and have been interpreted as deep melts of a mantle plume (Puffer, 2002); whereas other young basalt flows and dykes are more akin to mid-ocean ridge basalt (MORB) and have been explained as the result of a second stage of rifting and breakup (Cawood et al., 2001).

In NW Europe, the timing of CIMP magmatism is very similar. The oldest and most extensive magmatism is composed of basaltic dyke swarms at Egersund, Norway (616 ± 3 Ma; Bingen et al., 1998), the Tayvallich lavas and intrusive rocks in the Dalradian of Scotland (601 ± 4 Ma; Dempster et al., 2002; Fettes et al., 2011), and the Scandinavian Dyke Complex exposed in the Caledonian nappes (610–596 Ma; Baird et al., 2014; Gee et al., 2016; Root & Corfu, 2012; Svenningsen, 2001; Figure 1). The dyke complexes are postdated by ultramafic, mafic, and felsic plutons of the Seiland Igneous Province (580–560 Ma; Roberts et al., 2006), the Volyn LIP in eastern Europe (ca. 570 Ma; Shumlyanskyy et al., 2016), and several carbonatite and kimberlite complexes (590–520 Ma; Ernst & Bell, 2010, Torsvik et al., 2010). The parental magmas to the Seiland Igneous Province include picrites similar to OIB and are often explained as deep, hot mantle plume melts (e.g., Larsen et al., 2018), whereas the origin of the dominantly tholeiitic basalts of the dyke complexes is debated (Andréasson et al., 1998; Baird et al., 2014; Hollocher et al., 2007; Kirsch & Svenningsen, 2016).

3. The Scandinavian Dyke Complex

3.1. Nomenclature and Paleogeographic Origin

Dolerite dyke complexes are prominently outcropping in the Seve, Särv, and Corrovarre nappes of the Scandinavia Caledonides (Figure 1). They have been referred to as the Ottfjället dolerites (or Ottfjället dyke swarm) in the central part of Scandinavia (Hollocher et al., 2007) and the Sarek Dyke Swarm (Svenningsen,

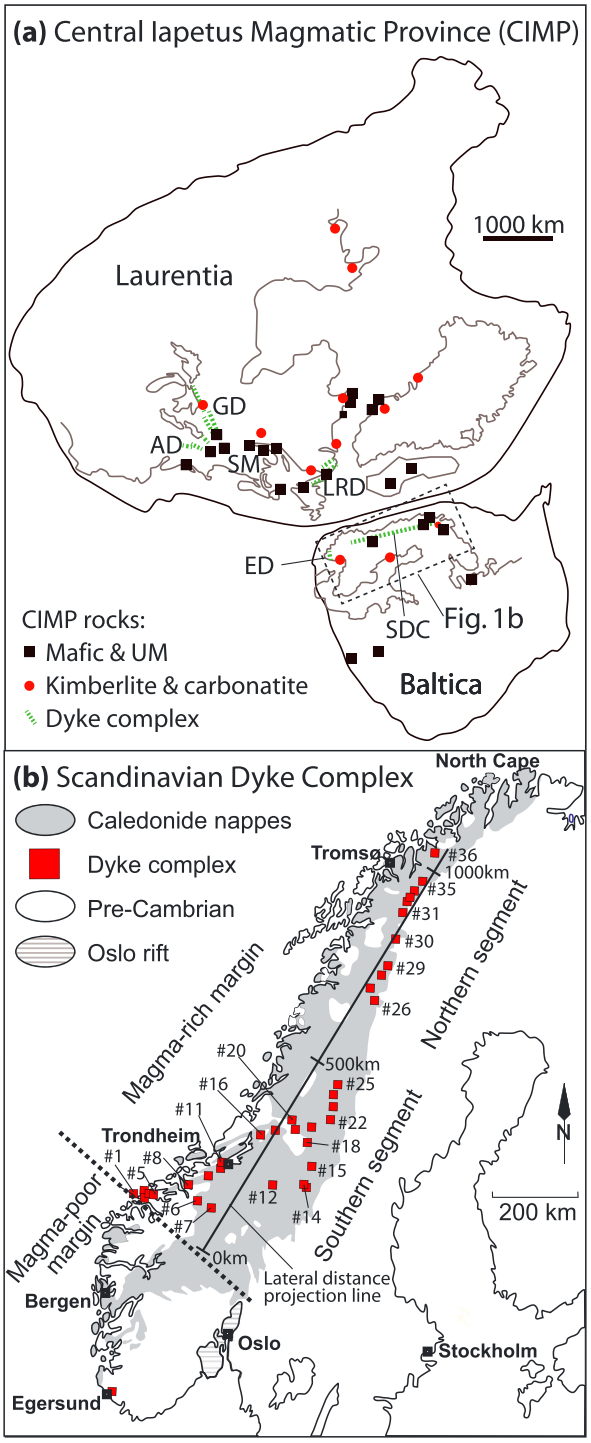

Figure 1. (a) Locations of magmatic rocks of the Central Iapetus Magmatic Province shown in a reconstruction of the Rodinia supercontinent (Li et al., 2008). Slightly modified from Ernst and Bell (2010) and Torsvik et al. (2010). (b) Map showing the Caledonian nappes of Scandinavia and the subdivision of the pre-Caledonian rifted margin of Baltica into a more than 1,000-km-long magma-rich margin in the north and a hyperextended magma-poor margin in the south (present frame of reference; Abdelmalak et al., 2015; Andersen et al., 2012). The locations of the 36 areas with outcrops of the SDC discussed in this contribution and for which we have compiled new and published geochemical data are shown and numbered in accordance with Table 1. Also shown is a distance line used to estimate the lateral position of the dyke areas from SW to NE. The midpoint of each area is projected orthogonally to the distance line. GD = Grenville Dyke Complex; AD = Adirondack Dyke Complex; LRD = Long Range Dyke Complex; ED = Egersund Dyke Complex; SDC = Scandinavian Dyke Complex; SM = Sutton Mountain triple junction.

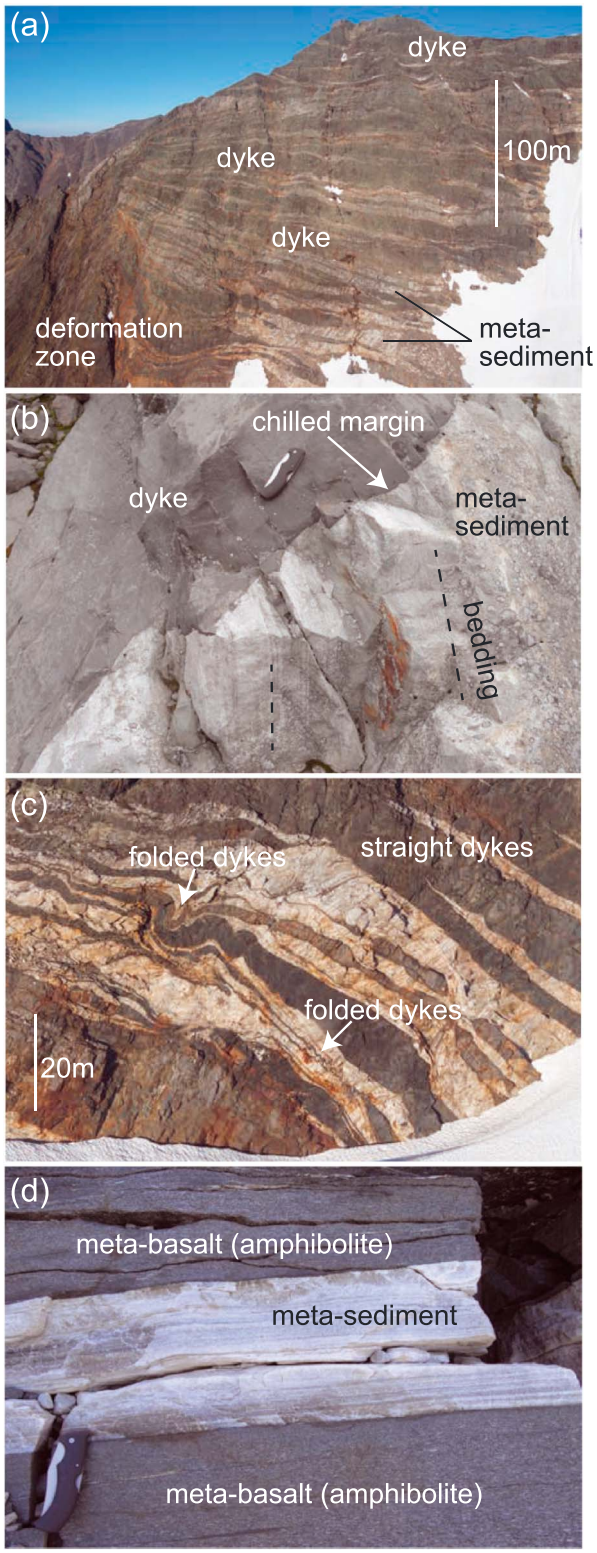

Figure 2. (a) Dyke swarm in the Sarek mountains showing undeformed dykes in the central and upper part of the cliff and a deformation zone the lower, left part of the outcrop. (b) Chilled margin of dyke cutting metasediments at a high angle to the original sedimentary bedding. (c) Gently folded and deformed dykes underlying straight and undeformed dykes. (d) Banded gneiss composed of amphibolite (metamorphosed dyke) and metasediment.

2001) and the Kebne Dyke Complex (Baird et al., 2014) in northern Sweden. The same dyke complex continues into northern Norway at Indre Troms and Corrovarre (Stølen, 1994; Zwaan & van Roermund, 1990). Andréasson et al. (1998) described the dykes as a coherent intrusive complex into sedimentary basins at the rifted margin of Baltica exceeding 1,000 km in length, and they used the term Baltoscandian Dyke Swarm. In this contribution we refer to these as the Scandinavian Dyke Complex.

The pre-Caledonian continental margin of Baltica formed during the Ediacaran and was closely associated with ~616–590 Ma breakup magmatism. Breakup and magmatism followed a long period (~200 Ma) of crustal extension and rifting of Rodinia in the Late Proterozoic (Nystuen et al., 2008). The margin constituted a more than 1,000-km-long magma-rich portion in the north which is the focus of this paper and further divided into southern and northern segments (see below) and a hyperextended magma-poor portion further to the south and not dealt with in this paper (present frame of reference, Figure 1; Abdelmalak et al., 2015; Andersen et al., 2012; Jakob et al., 2017). The origin of the dyke swarms either in the magma-rich rifted margin of Baltica or including outboard "exotic" terrains has been discussed. Kirkland et al. (2007) and Corfu et al. (2007) argued for the latter based on the geochronology of Neoproterozoic paragneisses and granitoids (610–980 Ma) that are cut by the dyke complexes and now part of the nappes of Finnmark in northernmost Scandinavia (Figure 1). Such basement ages are not found in situ in northernmost Scandinavia, and the nappes were therefore suggested to have an outboard origin. Other studies suggested that Middle Proterozoic Grenvillian and Sveconorwegian orogens continued north (present frame of reference) to East Greenland and as far as the Caledonides of Svalbard (e.g., Gee et al., 2016). This study and our recent work in the Ottfjället, Sarek, Kebnekaise, Indre Troms, and Corrovarre areas (Figure 1) support the traditional interpretation that these terranes and their dyke swarms are correlative, continuous, and of Baltican origin.

3.2. Field Relations

Many places such as Ottfjället, Sarek, Kebnekaise, Tornetrask, and Indre Troms (Figure 1) show spectacular outcrops of pristine magmatic dykes intruded into metasediments with cross-cutting relations and chilled margins (Figure 2 and Movie S1 of the supporting information). These outcrops constitute large (kilometer-size) low-strain lenses that have avoided Caledonian deformation and grade from essentially undeformed dykes and wall-rock metasedimentary hornfelses to strongly deformed and banded gneisses composed of amphibolite with or without garnet (i.e., metamorphosed mafic intrusions) and metasediments (Figure 2). The metamorphism ranges from well-preserved dykes with contact metamorphic wall-rock hornfelses to foliated amphibolite and locally eclogite facies tectonites (<750 °C and 7–14 kbar) formed during the Caledonian orogeny (Andréasson et al., 1998; Hollocher et al., 2007; Kullerud et al., 1990).

3.3. Is the Scandinavian Dyke Complex a LIP?

The dyke complex extends over 1,000 km in the Caledonian nappes (Figure 1), and the abundance of dykes ranges from 20 to >90% in well-exposed areas (Figure 2; e.g., Baird et al., 2014; Klausen, 2006; Roberts, 1990; Solyom et al., 1985; Stølen, 1994; Svenningsen, 1994). Although the original volume of magmatism is impossible to constrain due to the

Caledonian overprint and later erosion, a minimum volume may be estimated from present-day exposures. Klausen (2006) estimated the thickness and width of the Seve and Särv nappes to 4.5–6 and 80 km, respectively. If a minimum abundance of dykes is assumed to be 30% by volume and the minimum volume of the nappes is 1,000 km long, 80 km wide, and 5.3 km thick, the volume of dykes exceeds 0.13 Mkm^3. This minimum estimate, alone, fulfills the criteria for the size of a LIP (Bryan & Ernst, 2008). The short duration for the dyke emplacement discussed above also is similar to other LIPs (Bryan & Ernst, 2008).

4. Samples

To examine the lateral geochemical variations of the Scandinavian Dyke Complex, we have collected new dyke samples (n = 80) over four field seasons (2014–2017) along the length of the Scandinavian Caledonides (supporting information S1). In addition, we compiled all published geochemical data (n = 550; Table 1; supporting information S5). To ease the overview, the dyke outcrops were grouped into 36 geographical areas (typically one mountain area each) as shown in Figure 1 and listed in Table 1. The lateral distance measured from SW was estimated by projection of the midposition of each mountain area to a SW-NE line (Table 1 and Figure 1). We will also collectively refer to the mountain areas #26 to #36 as the northern segment and areas #1 to #25 as the southern segment (Figure 1).

The nature of the sampled rocks ranges from intrusive dykes with magmatic textures to garnet-bearing amphibolite gneiss and in one case eclogite (location #27, Table 1). The magmatic textures range from fine-grained basalt over dolerite to microgabbros that sometimes carry plagioclase and rare pyroxene phenocrysts.

5. Methods

The whole rock compositions of 80 samples were measured at Bureau Veritas Commodities Canada Ltd. by X-ray fluorescence (major elements) and by inductively coupled plasma-mass spectrometry (trace elements) and are reported in supporting information S2. Analyses of certified reference materials show that the relative deviation from the reference values are less than 1% for the major elements, less than 4% for P_2O_5, and less than 7% for the trace elements discussed in this paper (supporting information S3). Repeat analyses of samples demonstrate reproducibility within 1.4% for the major elements, within 8% for MnO and P_2O_5, and within 14% for the trace elements discussed in this paper, with one exception at 40% (Th) in one sample with low concentrations (supporting information S4).

The older published geochemical data were mainly analyzed by X-ray fluorescence (XRF) and instrumental neutron activation, providing major element and some trace element compositions (Andréasson et al., 1979; Beckholmen & Roberts, 1999; Kathol, 1989; Pettersson, 2003; Solyom et al., 1979, 1985; Stølen, 1994; Svenningsen, 1994). The more recent data sets include full trace elements by inductively coupled plasma mass spectrometry (ICP-MS) (Baird et al., 2014; Hollocher et al., 2007; Kirsch & Svenningsen, 2016; Svenningsen, 1994). Supporting information S5 lists the compiled data.

The Sr isotope composition of plagioclase phenocrysts were measured in situ in nine samples by laser-ablation multicollector inductively coupled plasma mass spectrometry at Aarhus Geochemistry and Isotope Research Platform, Aarhus University. Numerous studies have recently published accurate and precise plagioclase Sr data measured by laser-ablation multicollector inductively coupled plasma mass spectrometry (e.g., Kimura et al., 2013; Ramos et al., 2004; Wilson et al., 2017). Our analyses were done on ~1-cm-thick rock billets, with laser spot placement guided by micro-XRF petrography. The method employed is described in detail in supporting information S6 and summarized here: A 193-nm excimer laser (Resonetics RESOlution) was used to ablate 154-μm-diameter spots, with the ablated material carried in a He + Ar carrier gas to a Nu Plasma II multicollector inductively coupled plasma mass spectrometry. Data were reduced with corrections for Kr, CaAr, and Rb isobaric interferences on the Sr isotopes. A rock glass bracketing standard (BCR-2) was used to correct the offset between Sr and Rb mass bias factors and Rb-Sr element fractionation (to ensure an accurate age correction). Interference-corrected $^{87}Sr/^{86}Sr$ ratios were normalized to an in-house bytownite standard. Measurements of an additional in-house standard (fused plagioclase) yielded $^{87}Sr/^{86}Sr = 0.704716 \pm 0.000071$ (2 standard deviation; n = 10), in agreement with a reference value of 0.704701 ± 0.000016 (based on solution multicollector

Table 1
Overview of Compiled Samples and Their Locations

Country	Region	Location names	Location #	Position km	No. of analyses Th/Nb < 0.15	No. of analyses Th/Nb ≥ 0.15	References
N	Møre og Romsdal	Lepsøy	1	18	18	1	Hollocher et al. (2007)
N	Møre og Romsdal	Brattvåg and Sunnaland	2	22	4		Hollocher et al. (2007)
N	Møre og Romsdal	Tennøy, Lauvøy, and Skår	3	31	12	1	Hollocher et al. (2007)
N	Møre og Romsdal	Otrøy, Midøy, and Dryna	4	35	10	1	Hollocher et al. (2007)
N	Møre og Romsdal	Dragneset and Øygardsneset	5	40	7		Hollocher et al. (2007)
N	Trøndelag	Driva and Oppdal	6	91	14		Solyom et al. (1985)
N	Trøndelag	Oppdal	7	94	15		Hollocher et al. (2007)
N	Møre og Romsdal	Åsbøen, Ura, and Årnes	8	109	11		Hollocher et al. (2007)
N	Møre og Romsdal	Vasslivatnet	9	149	4		Hollocher et al. (2007)
N	Trøndelag	Orkanger	10	178	30		Hollocher et al. (2007); Solyom et al. (1985)
N	Trøndelag	Ystland, Geita, and Kjøra	11	184	15		Hollocher et al. (2007)
S	Jämtland	Sylarna	12	204	46		Solyom et al. (1985); Pettersson (2003)
S	Jämtland	Lunndörs-, Anaris-, and Ott-fjällene	13	225	9		This study
S	Jämtland	Lunndörs-, Anaris-, and Ott-fjällene	14	233	154		Solyom et al. (1985, 1979)
S	Jämtland	Alsen	15	280	12		Solyom et al. (1985)
N	Trøndelag	Leksdalsvann	16	290	14		Andréasson et al. (1979)
N	Trøndelag	Leksdal	17	315	31		Solyom et al. (1985)
S	Jämtland	Ansætten	18	326	9		Solyom et al. (1985)
N	Trøndelag	Turtbakktjørna	19	339	6		Solyom et al. (1985)
N	Trøndelag	Snåsa-Lurudal	20	351	6		Solyom et al. (1985)
N	Trøndelag	Sørli	21	360	13	1	Beckholmen and Roberts (1999)
S	Jämtland	Strøms-Vattudal	22	396	6		Solyom et al. (1985)
S	Jämtland	Storsjauten	23	422	7		Solyom et al. (1985)
S	Jämtland	Borgahällen and Dabbsjön	24	444	10		Solyom et al. (1985)
S	Lappland	Kultsjøen	25	471	2		Solyom et al. (1985)
S	Lappland	Piesa	26	675	2		Solyom et al. (1985)
S	Lappland	Tsäkkok	27	709	11		This study; Kullerud et al. (1990)
S	Lappland	Pårte, Sarek National Park	28	734	8	1	This study
S	Lappland	Äpar and Favorithällen, Sarek National Park	29	758	23		Svenningsen (1994)
S	Lappland	Äpar and Sarektjåkka, Sarek National Park	29	758	9	4	This study
S	Lappland	Kebnekaise	30	822	20	4	This study; Kirsch and Svenningsen (2016); Baird et al. (2014)
S	Lappland	Nissosnoukki, south of Tornetrask	31	867	2		This study
S	Lappland	Vaivvancohkka, north of Tornetrask	32	887	8	5	This study; Kathol (1989)
N	Troms	Rohkunborri, Jounnetcohkat, and Kistufell	33	902	21	2	This study; Stølen (1994)
N	Troms	Njumis and Høgskardet	34	925	16	2	This study; Stølen (1994)
S	Lappland	Tjuotjmer	35	956	2	2	This study
N	Troms	Corrovarre	36	1072	19		This study; Roberts (1990)
	Total				606	24	

Note. N = Norway; S = Sweden.

inductively coupled plasma mass spectrometry measurements of four different fragments). The $^{87}Sr/^{86}Sr$ for rock standards with $^{87}Rb/^{86}Sr$ up to 0.066 were also reproduced accurately, and only analyses of plagioclase with $^{87}Rb/^{86}Sr < 0.066$ are reported here (4 of 81 analyses had $^{87}Rb/^{86}Sr > 0.066$). The Sr isotope data are reported in supporting information S7.

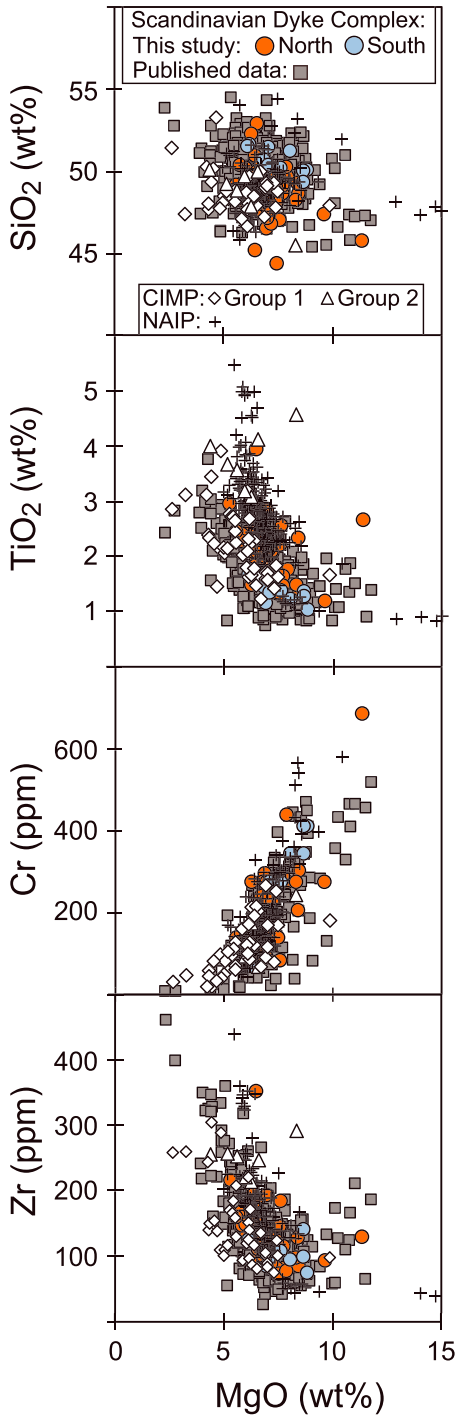

Figure 3. Compositions of the Scandinavian Dyke Complex for the compiled data set screened for crustal contamination (24 samples with Th/Nb > 0.15 are excluded) totaling 606 analyses. New data (n = 80) in supporting information S2 and published data (n = 550) in supporting information S5. Also shown are (i) flood basalts of the Northeast Atlantic Igneous Province (NAIP) from the 6-km-thick volcanic pile in East Greenland (Tegner et al., 1998); (ii) group 1 tholeiitic dykes of the Central Atlantic Magmatic Province (CIMP) in northeast America (Ernst & Buchan, 2010; Seymour & Kumarapeli, 1995; Volkert et al., 2015); and (iii) group 2 CIMP dykes in the Sutton mountains of northeast America referred to as Laurentian ocean island basalt (Puffer, 2002).

6. Results

6.1. Major and Trace Element Compositions

The new data set for the Scandinavian Dyke Complex defines a coherent suite of tholeiitic ferrobasalt with 5–11 wt% MgO, 44–53 wt% SiO_2, and 9–16 wt% FeO_{tot} (Figure 3, supporting information S2). The TiO_2 (1.0–4.0 wt%) and Zr (72–350 ppm) increase, and Cr (684–68 ppm) decreases with decreasing MgO (Figure 3), consistent with a control by fractional crystallization. The new data set is similar to the compiled data set also shown in Figure 3. In a multielement diagram, the incompatible trace element compositions of dykes from the northern segment form largely flat patterns from the least (right side) to the most (left side) incompatible elements (Figure 4). The compositional variation is relatively high for K, U, Ba, and Rb; this can probably be ascribed to alteration and/or metamorphic effects. Although the rocks range from magmatic (dolerite) to metamorphic (garnet amphibolite; Figure 2), there are no significant differences of the elements used in this contribution between the two rock types in the Sarek area where they can be compared (supporting information S8). The trace element patterns of the southern segment, in contrast, generally increase from right to left and also show increased variation for K, U, Ba, and Rb.

6.2. Sr Isotope Composition

The Sr isotope composition in plagioclase phenocrysts from nine samples are shown in Figure 5. The southern (five samples) and northern (four samples) segments of the dyke complex define two fields with lower bounds for initial (615 Ma) $^{87}Sr/^{86}Sr_i$ of 0.7033 and 0.7025 (one point at 0.7024), respectively. The scatter within each sample toward higher values is considerable. However, the plagioclase $^{87}Sr/^{86}Sr_i$ is not correlated with bulk rock Th/Nb.

7. Analyses of Geochemical Variations

7.1. Assessment of Crustal Contamination

The present contribution focuses on mantle processes, and we have, therefore, first assessed the potential role of crustal contamination. High Th/Nb is a hallmark of continental crust (0.47; Albarède, 2003). This ratio is little affected by mantle melting and fractional crystallization as Nb and Th are almost equally incompatible. Moreover, Th and Nb are available in most of the sample sets compiled here. We have excluded samples (n = 24) with Th/Nb >0.15, resulting in a final data set with 606 samples that will be used throughout this contribution (Table 1). The role of crustal contamination can also be assessed in a diagram of Th/Yb versus Nb/Yb that Pearce (2008) used to distinguish an array of melts formed from mantle sources in the oceans (far away from continental crust; Figure 6a). In this diagram, the average compositions, calculated for the dykes in each area, the screened data set falls within the oceanic mantle melt array or straddles the upper bound. Also shown are the samples with Th/Nb >0.15 and two mixing curves between MORBs and average continental crust indicating that most of these samples have assimilated 5% to 30% continental crust. This analysis demonstrates that the screened data set reflects melting of mantle sources akin to those of the ocean basins, although minor crustal contamination cannot be ruled out. Below, the Sr isotope data show contamination of some samples in the screened data set (<7%

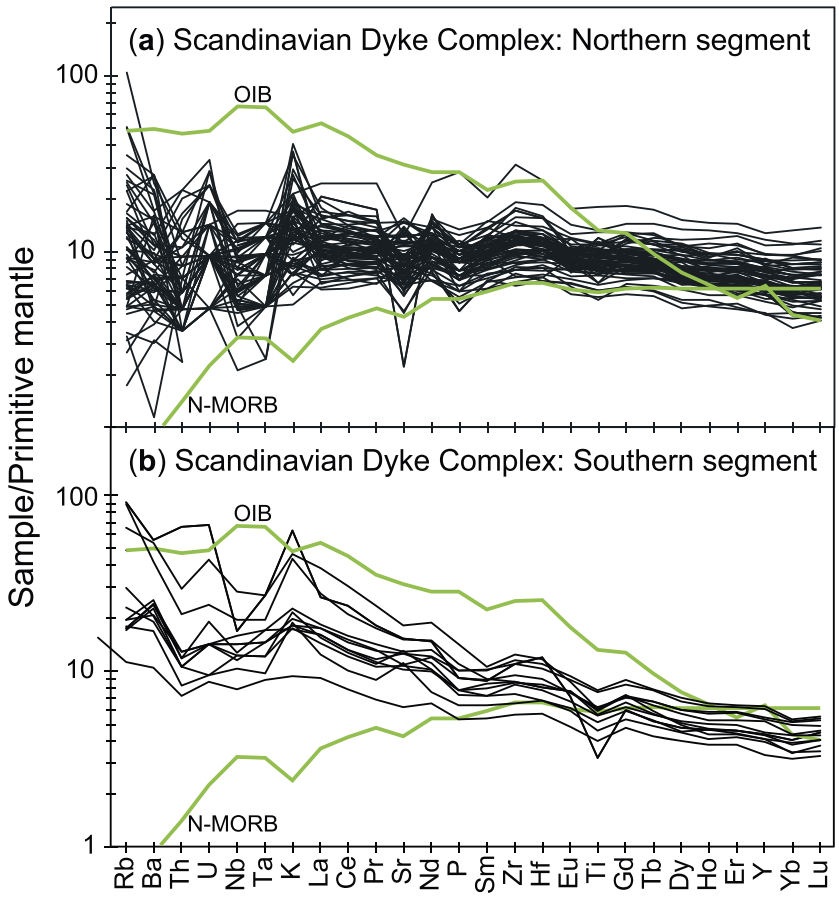

Figure 4. Multielement diagram showing the new data of this study for samples of the northern segment (a) and of the southern segment (b) of the Scandinavian Dyke Complex. The elements are arranged with increasing incompatibility in mantle rocks from right to left and are normalized to primitive mantle (Sun & McDonough, 1989). Also shown are normal mid-ocean ridge basalt (N-MORB) and ocean island basalt (OIB; Sun & McDonough, 1989).

crust, section 7.3). Such crustal contamination will not change the results of the following analysis of mantle dynamics.

7.2. Lateral Geochemical Zoning

The ΔNb value of basaltic rocks is a proxy for Nb enrichment of the mantle source. The ΔNb notation was defined for the present-day North Atlantic where Fitton et al. (1997) demonstrated that in a log-log plot of Nb/Y versus Zr/Y, the basaltic rocks from Iceland defined a compositional field that was relatively enriched in Nb and separated from the compositions of normal MORB away from Iceland. They defined the ΔNb as

$$\Delta\mathrm{Nb} = 1.74 + \log(\mathrm{Nb/Y}) - 1.92(\mathrm{Zr/Y}). \quad (1)$$

This equation results in positive values for basalts that are geochemically enriched in Nb (i.e., similar to Iceland) and negative values for samples that are relatively depleted. Following Fitton et al. (1997), basalts with positive and negative ΔNb can be explained as originating from mantle sources enriched and depleted in Nb, respectively. The ΔNb notation is particularly useful in the present study for two reasons. First, it is based on trace elements that are relatively immobile (Pearce, 2008) and therefore are expected to be changed minimally during metamorphic reactions (supporting information S8). Second, the elements Nb, Zr, and Y are well determined by X-ray fluorescence and instrumental neutron activation methods and are therefore available in the older, published data sets.

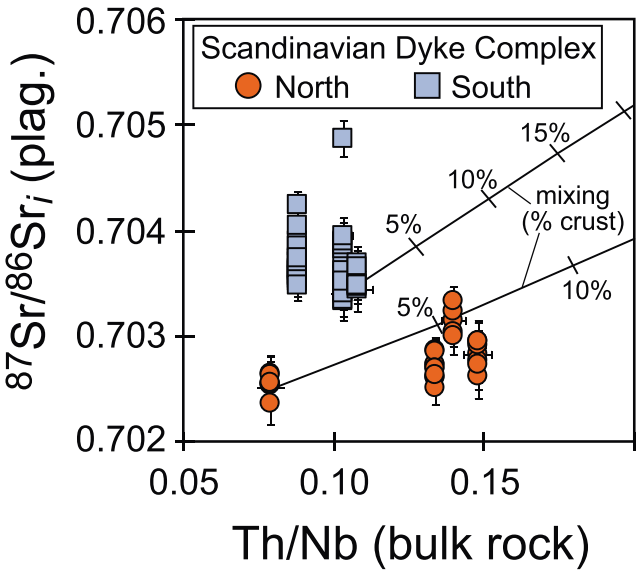

Figure 5. Initial (615 Ma) $^{87}Sr/^{86}Sr_i$ in plagioclase phenocrysts versus whole rock Th/Nb in five dykes from the southern segment and four dykes in the northern segment of the Scandinavian Dyke Complex. Each data point represents a single laser ablation analysis. Methods and data are given in supporting information S6 and S7.

Figure 7a shows the variation in ΔNb of the dykes along >1,000 km of Scandinavian nappes and showing average values for our new data set and for the published data set (Table 1 and Figure 1). In both data sets, the southern segment has positive ΔNb reaching values up to +0.59 between 300 and 500 km; that is, Nb is enriched 5.9 times relative to ΔNb of zero for a given Zr/Y (Fitton et al., 1997). The northern segment (675–1,075 km) has lower ΔNb and shows a northward decreasing trend with negative values down to −0.23 (Figure 7a).

Other trace elements such as the rare earth elements are only available in the present data set, and in the more recently published data sets (Baird et al., 2014; Hollocher et al., 2007; Kirsch & Svenningsen, 2016; Svenningsen, 1994). Figure 7b shows the variation in the slope of a light rare earth element (La) relative to a middle rare earth element (Sm) normalized to chondrite (La/Sm_N). The available La/Sm_N data also show pronounced lateral differences in both data sets from elevated values (1.35 to 2.10) in the southern segment to lower values in the northern segment (0.87–1.47). This is consistent with the trace element patterns shown in Figure 4. A positive correlation of La/Sm_N and ΔNb (Figure 8) in both data sets confirms the lateral zoning in incompatible elements from enriched basaltic compositions in the southern segment to more depleted compositions in the northern segment.

7.3. Sr Isotopic Composition of the Mantle Sources

The reported Sr isotope composition in plagioclase phenocrysts shows the plagioclase $^{87}Sr/^{86}Sr_i$ is not correlated with bulk rock Th/Nb (Figure 5). The generally higher $^{87}Sr/^{86}Sr_i$ of the southern segment (lower bound of 0.7033), therefore, cannot be explained by a greater degree of crustal contamination than the basalts of the northern segment (lower bound of 0.7025). The scatter within segment is considerable but can partly be explained by up to 7% crustal contamination, as indicated by mixing lines between low $^{87}Sr/^{86}Sr_i$ basalt end members and continental crust (Figure 5). We also note that crustal contamination is much more prevalent in the northern segment, for example, with a higher frequency of samples with Th/Nb >0.15 relative to the southern segment (Table 1 and supporting information S2 and S5). Nevertheless, plagioclases from three of the four samples from the north have $^{87}Sr/^{86}Sr_i$ that are indistinguishable within error and appear to have been minimally contaminated. Fluids related to Caledonian metamorphism and/or weathering may have disturbed the Rb-Sr systematics, although there is no indication of elemental disturbance (supporting information S8). Moreover, such effects are avoided by analyzing Sr isotopes in unaltered plagioclase phenocrysts, instead of bulk rocks. We therefore conclude that crustal contamination (<7%) is recorded by some plagioclase phenocrysts, but the least radiogenic plagioclase grains show that the magmas and, therefore, the mantle source of the southern segment were enriched ($^{87}Sr/^{86}Sr_i$ ~0.7033) relative to the northern segment ($^{87}Sr/^{86}Sr_i$ ~0.7025). This is corroborated by bulk rock $^{87}Sr/^{86}Sr_i$ of 0.7028 ± 0.0002 reported for the Corrovarre dykes in the north (area 36, Figure 1) and 0.7037 ± 0.0003 for the Ottfjället dykes in the south (location 14, Figure 1; Bingen & Demaiffe, 1999; Zwaan & van Roermund, 1990).

8. Geochemical Modelling of Mantle Sources and Temperature

To constrain the possible mantle melting dynamics, mantle potential temperature (T_P), and source lithologies that can explain the observed compositions of the Scandinavian Dyke Complex, we present the results of new mantle melting models. We apply both major and trace element modelling. In particular, we seek explanations for the described geochemical zoning in ΔNb, La/Sm, and $^{87}Sr/^{86}Sr$ from south to north of the magma-rich margin (Figures 5 and 7).

8.1. Major Element Modelling

The major element compositions of primitive basalts can provide constraints on mantle potential temperature, T_P (e.g., Herzberg et al., 2007). Notably, such constraints are independent of those derived from the

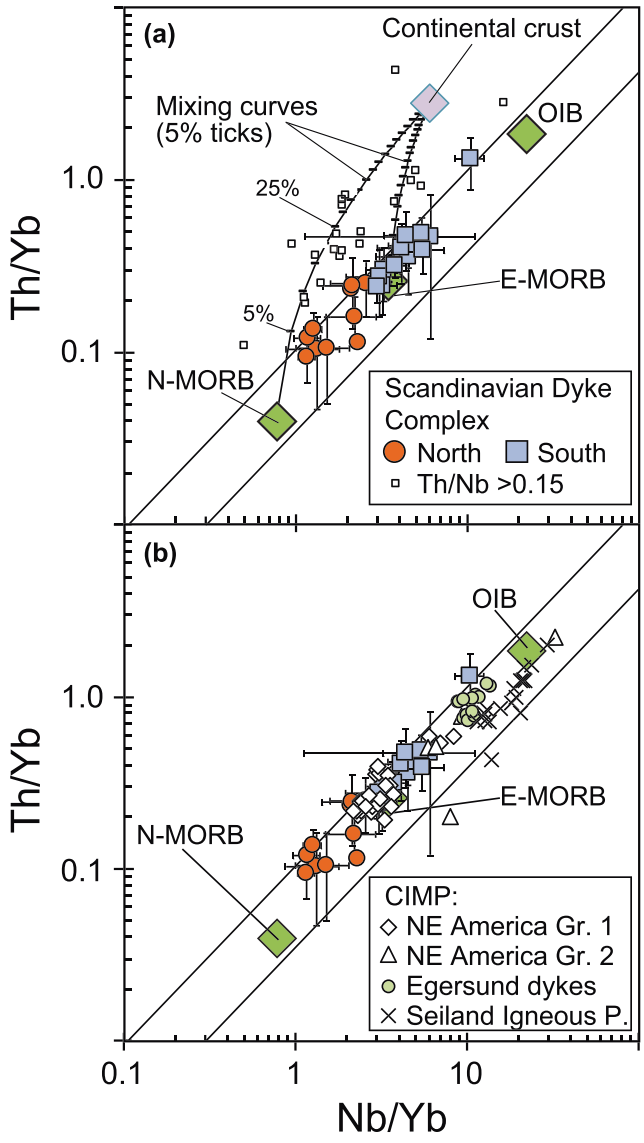

Figure 6. (a) Th/Yb versus Nb/Yb showing the average compositions for the 37 locations of the Scandinavian Dyke Complex (Figure 1 and Table 1); symbols are separated into southern and northern segments of the magma-rich margin. The average compositions are based on 606 samples screened for crustal contamination (Th/Nb < 0.15). The remaining 24 samples judged to be crustally contaminated (Th/Nb ≥ 0.15) are also plotted as individual points. The oceanic mantle array is from Pearce (2008), and the compositions of depleted mid-ocean ridge basalt (normal mid-ocean ridge basalt [N-MORB]), enriched mid-ocean ridge basalt (E-MORB), and ocean island basalt (OIB) are from Sun and McDonough (1989). Average continental crust is from Albarède (2003). The two lines with 5% tick marks illustrate mixing of continental crust with N-MORM and E-MORB. (b) Th/Yb versus Nb/Yb for other rocks of the Central Iapetus Magmatic Province (CIMP): NE American tholeiites (group 1: Ernst & Buchan, 2010; Volkert et al., 2015); NE American Laurentian OIB (group 2: Puffer, 2002); Egersund dykes (Bingen & Demaiffe, 1999); and Seiland Igneous Province alkali-basalt dykes (Reginiussen et al., 1995).

forward trace element modelling discussed below. Here we apply the thermobarometer of Lee et al. (2009) that, based on an extensive parameterization of experimental data, provides estimates for the temperature and pressure of final melt segregation from olivine + pyroxene-bearing mantle sources. This thermobarometer is based primarily on the inverse relationship between pressure and the melt SiO_2 content (Carmichael, 2004) and the positive correlation of temperature and melt MgO content (Lee & Chin, 2014). Application of this thermobarometer to evolved basalts requires that the composition of the evolved melt is controlled by olivine fractionation alone. Thus, the program first estimates the primary melt composition by adding olivine until the melt is in equilibrium with a given mantle olivine composition, which we assume has an Mg#, that is, Mg / (Mg + Fe), of 0.91. The equilibrium temperature and pressure of this primary melt composition are subsequently constrained by the parameterization. Conveniently, both calculations are performed using the Excel spreadsheet provided by Lee et al. (2009). Following Lee et al. (2009), T_P is then calculated by (a) back-projecting the equilibrium temperature and pressure to the peridotite solidus along a melting path parameterized using the model of Katz et al. (2003) and (b) then finding T_P as the potential temperature of the mantle adiabat that intersects the solidus at this pressure and temperature.

Similar to Lee et al. (2009), we assume that only samples of the Scandinavian Dyke Complex with more than 8.5 wt% MgO can be assumed to be largely controlled by olivine fractionation. Due to the possible increase in SiO_2 of the magmas as a consequence of crustal assimilation, we only consider samples with Th/Nb < 0.15 as discussed above. Using these criteria, the major element composition of 39 samples was entered into the spreadsheet, and 32 of these yielded temperature and pressure estimates for final melt segregation in the mantle source. These temperatures range from 1,382 to 1,652 °C and the pressures from 1.3 to 5.0 GPa as shown in supporting information S13. The corresponding T_Ps range from 1,436 to 1,584 °C for the entire data set (supporting information S13), and the kernel density distribution (n = 32) is shown in Figure 9. The samples that gave T_P estimates are distributed over the entire dyke swarm (12 locations in the southern segment and 2 locations in the northern segment; Table 1 and Figure 1) and exhibit a Gaussian density distribution with a top at 1,498 °C, but with four outliers close to 1,580 °C. We conclude that the major element thermobarometer consistently yields mantle potential temperatures significantly above ambient mantle (ΔT_P of 100–250 °C), with a maximum density just below 1,500 °C (ΔT_P of 170 °C). A significant difference between T_P of the southern and northern segments cannot be discerned.

8.2. Trace Element Modelling

We modeled the compositions of basaltic melts produced by melting dynamically upwelling mantle using the REEBOX PRO application (Brown & Lesher, 2016). This forward model calculates the composition of the incompatible lithophile trace elements in mantle melts using the latest thermodynamic and experimental constraints on melting reactions and mineral-melt partitioning coefficients and can simulate passive and active upwelling scenarios, melting of several potential mantle lithologies and allows for exploring variable T_P. The model assumes incremental batch (i.e., near-fractional) melting of the upwelling mantle. This is simulated in a stepwise fashion where the melting column is subdivided into a finite number of decompression steps

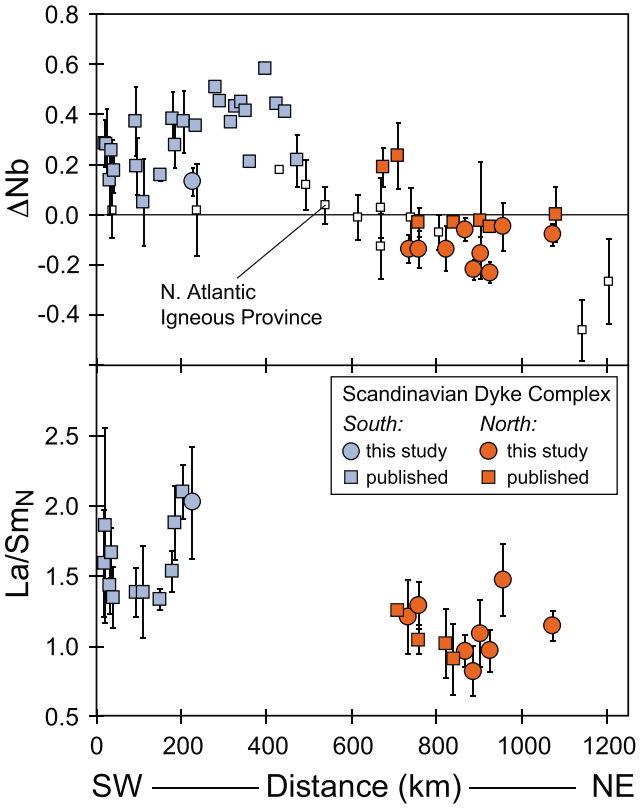

Figure 7. SW to NE compositional variation in the Scandinavian Dyke Complex. (a) ΔNb (1 s.d. error bars) showing average values for our new data set and for the published data set for 36 locations (Figure 1 and Table 1). Also shown are lateral variations in ΔNb of the North Atlantic Igneous Province with radial distance from the assumed center of the proto-Icelandic mantle plume (Fitton et al., 1997). To fit the scale used here, 350 km is subtracted from the published distances to the plume center; (b) La/Sm$_N$ for 22 locations where inductively coupled plasma mass spectrometry data are available (Baird et al., 2014; Hollocher et al., 2007; Kirsch & Svenningsen, 2016; Svenningsen, 1994; this study).

between the solidus and the base of the nonmelting lithosphere. Each small decompression step involves melting and instantaneous removal of the melt and recalculation of the trace element composition of the residual mantle. The instantaneous melt composition is calculated using the equation for nonmodal batch melting, and the composition of the residual mantle is calculated by mass balance (Brown & Lesher, 2016). In the next decompression step, the previous residual mantle parcel moves up to slightly lower pressure (simulating upwelling) and melts again, producing a slightly more depleted residual mantle and so forth. All instantaneous melts generated within the melting region are pooled together to form an aggregate melt composition (e.g., equation 12 in Brown & Lesher, 2016). We assume the 2-D shape of the melting region is triangular (apex at the top) where melting takes place in upwelling mantle parcels but stops when convection turns to horizontal; it is therefore often referred to as the corner-flow model initially developed to simulate melting dynamics at mid-ocean spreading ridges (Plank & Langmuir, 1992) but appears applicable also to the formation of LIPs associated with continental rifting (Brown & Lesher, 2016). Melting begins at the solidus intersection with the mantle adiabat (specified by its T_P), and the maximum degree of melting (F_{max}) is obtained at the upper apex of the melting region. In the triangular melting region, the average degree of melting ($F_{average}$) for the pooled melt is given by equation 28 of Brown and Lesher (2016).

A key factor for the composition of melts produced by dynamically upwelling peridotite mantle is the transition from garnet to spinel stability. In REEBOX PRO, garnet is stable on the pyrolite peridotite solidus at pressures above 2.7 GPa, whereas spinel is stable below 3 GPa (Brown & Lesher, 2016), producing a 0.3-GPa transition where both phases exist. Garnet preferentially holds back the heaviest rare earth elements, and this effect is best monitored by the ratio of a middle rare earth element (Dy) to a heavy rare earth element (Yb) normalized to chondrite (Dy/Yb$_N$). A plot of Dy/Yb$_N$ versus La/Sm$_N$ (Figure 10) therefore relates to the garnet effect on the y axis and mantle source composition and degree of melting (Tegner et al., 1998) on the x axis, assuming a homogeneous peridotite source. The effects of fractional crystallization and crustal contamination are largely negligible in this diagram; both Dy/Yb$_N$ and La/Sm$_N$ are unrelated to a fractionation index such as MgO (supporting information S9) and to the Th/Nb proxy for crustal contamination (supporting information S10).

The data for the southern and northern segments plot in two fields in Figure 10 with higher La/Sm$_N$ (1.4–2.1) in the southern segment compared to the northern segment (0.9–1.5); both segments have about the same range in Dy/Yb$_N$ (1.16–1.33). These values are compared to model results for melting-enriched mantle (primitive mantle; McDonough & Sun, 1995) at T_P from ambient mantle (1,330 °C) to 1,630 °C, that is, ΔT_P of 0 to 300 °C (Figure 10a). The result of increasing ΔT_P is increasing Dy/Yb$_N$ values; this is the consequence of the garnet effect due to deeper intersection of the mantle solidus at higher T_P. The compositions of dykes in the southern segment are well explained by model melts of primitive mantle for average degrees of melting from 3% to 10% and ΔT_P ranging from 75 to 150 °C; these values are similar to estimates for basalts formed in other LIPs (Brown & Lesher, 2014; Herzberg & Gazel, 2009; Tegner et al., 1998). The more depleted compositions of the northern segment can only be fit by the model melts of primitive mantle at very high ΔT_P (>200 °C) and more than 12% average melting. In contrast, the dyke compositions of the northern segment are better explained by model melts assuming a depleted mantle source (depleted MORB mantle of Salters & Stracke, 2004; Figure 10b). The data fall between model curves for ΔT_P ranging from 75 to 150 °C, suggesting average degrees of melting from 3% to 6%. In theory, it is also possible to explain the more

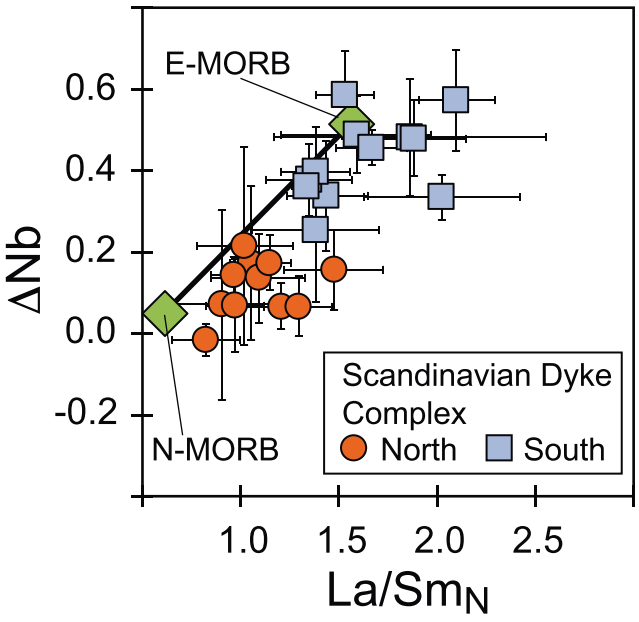

Figure 8. Average ΔNb vs La/Sm$_N$ (1 s.D. error bars) for the Scandinavian dyke complex; symbols separated into southern and northern segments. Shown are 23 locations where inductively coupled plasma mass spectrometry data are available (Baird et al., 2014; Hollocher et al., 2007; Kirsch & Svenningsen, 2016; Svenningsen, 1994; this study). Also shown are the compositions of N-MORB and E-MORB (Sun & McDonough, 1989). N-MORB = normal mid-ocean ridge basalt; E-MORB = enriched mid-ocean ridge basalt.

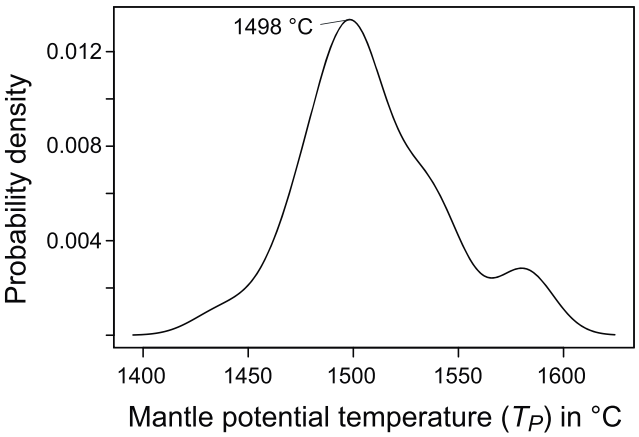

Figure 9. Gaussian kernel density distribution of mantle potential temperature (T_P) calculated for samples of the Scandinavian Dyke Complex ($n = 32$). The final equilibrium temperature and pressure of the magmas in the mantle were calculated using the major element thermobarometer of Lee et al. (2009) and converted to T_P using the method described in the text. The T_P of the entire data set, covering 14 locations in both the southern and northern segments, exhibits a Gaussian density distribution with a top at 1,498 °C, but with four outliers close to 1,580 °C. The calculations were restricted to largely uncontaminated (Th/Nb < 0.15) and primitive samples that contained more than 8.5 wt% MgO. The data are listed in supporting information S13. The kernel density estimations follow the method discussed in Rudge (2008) and were calculated using the Free Statistics Software of Wessa (2015).

enriched compositions of the southern segment by melting depleted mantle at moderate ΔT_P (50–75 °C), although this would require very low average degrees of melting (<3%; Figure 10b). Such low degrees of melting, however, are not likely to produce the tholeiitic major element compositions of the southern dykes (Figure 3). Likewise, ΔNb and Sr isotopes (Figures 5–7) are also best explained by a lateral change from an enriched mantle source in the south and a depleted mantle source in the north.

8.3. Summary of Geochemical Modelling

We conclude that the lateral compositional changes in the rare earth element compositions of the dyke complex (Figures 4, 7, 8, and 10) are best explained by melting mantle that was anomalously hot relative to ambient mantle (ΔT_P of 75–150 °C). Elevated T_P is independently confirmed by the major element modelling yielding ΔT_P of 100–250 °C with no discernable difference between the southern and northern segments (Figure 9). The rare earth element modelling shows the melting domain is best explained if it was zoned with enriched lithologies and compositions (primitive mantle) under the southern segment and depleted lithologies and compositions (depleted MORB mantle) under the northern segment. This interpretation is corroborated by the Sr isotope compositions (Figure 5).

Mantle warming due to long-term thermal insulation by continental lithosphere can produce ΔT_P up to 100 °C (Coltice et al., 2007; Herzberg & Gazel, 2009) and therefore does not provide a fulfilling explanation for the modeled temperatures. Moreover, the distinct compositional zoning in trace elements and Sr isotopes (Figures 4, 5, 7, and 8) and the basalt compositions similar to the oceanic mantle array (Figure 6) favor an explanation by upwelling of a zoned mantle plume akin to Iceland today and to the NAIP ca. 56 Myr ago (Fitton et al., 1997). Analogue and computational modelling supports the view that mantle plumes may be laterally zoned on a length scale of 1,000 km with a compositionally enriched central portion and a more depleted outer margin (Jones et al., 2016).

9. A 615 Ma Plate Reconstruction of Baltica and Laurentia

Two LLSVPs (Garnero et al., 2007) today exist at the core-mantle boundary beneath Africa (dubbed TUZO) and the Pacific (JASON). Using hybrid mantle frames (combination of moving hot spot and true polar wander (TPW)-corrected paleomagnetic frames), it has been argued that the LLSVPs have been stable for at least 300 Myr with deep plumes sourcing LIPs (Figure 11a) and kimberlites mostly from their margins (Torsvik et al., 2014, 2016). That remarkable correlation between surface volcanism and deep mantle features potentially provides a novel and quantitative way to derive "absolute" plate motions in a mantle reference frame before Pangea. This approach assumes that TUZO and JASON have remained nearly stationary before Pangea time and that the origin of mantle plumes can be tied to their edges. These views are, however, far from being universally accepted and have generated debate in the geophysical literature. We will therefore briefly review some of the pros and cons for this assumption here.

9.1. Stability and PGZs of LLSVPs

That plumes mainly form at the margins of the LLSVPs and that they are approximately stable through time have wide implications and have

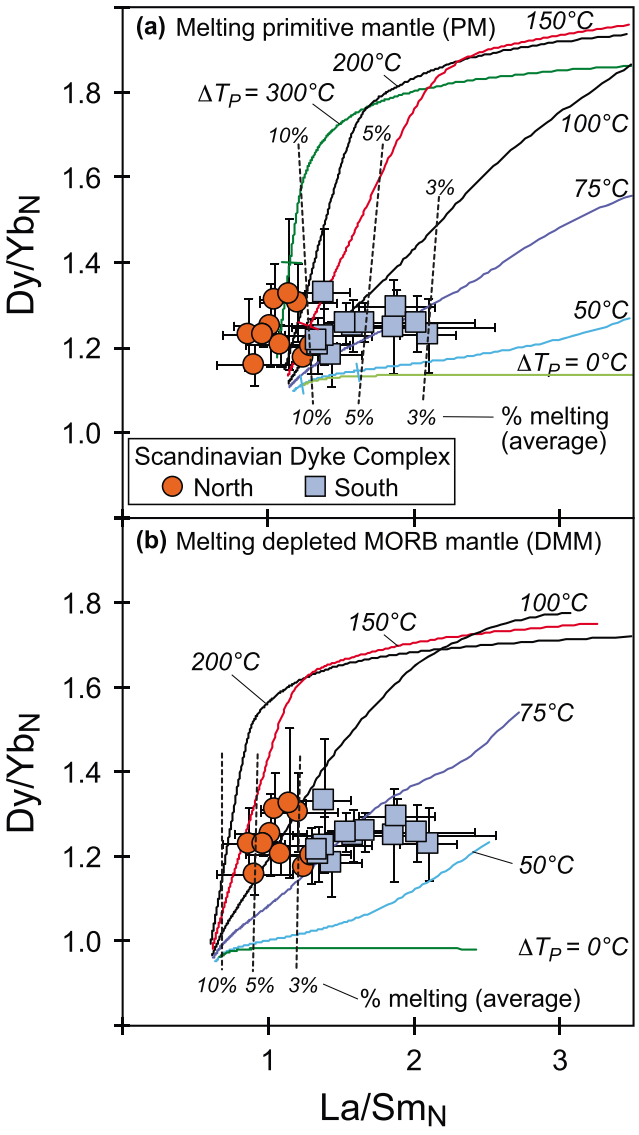

Figure 10. Dy/Yb_N versus La/Sm_N of the Scandinavian Dyke Complex; symbols separated into southern and northern segments. (a) Forward model melts produced by melting primitive mantle (McDonough & Sun, 1995) at mantle potential temperatures from 1,330 to 1,630 °C, that is, up to 300 °C above ambient mantle. (b) Forward model melts produced by melting depleted MORB mantle (Salters & Stracke, 2004) at the same mantle potential temperatures as in (a). Modelling based on REEBOX PRO (Brown & Lesher, 2016), see text. MORB = mid-ocean ridge basalt.

promoted a number of numerical modelling experiments to reproduce and explain (or reject) these features. Among the most avid opponents are those who deny the very existence of mantle plumes, mantle modelers disagreeing with the interpretation of LLSVPs as mantle structures with distinct chemical properties (e.g., Davies et al., 2015), and those suggesting that LLSVPs are highly mobile and simply shaped and destroyed by sinking slabs (e.g., Flament et al., 2017).

Numerical models of mantle convection have been used to investigate the stability of the LLSVPs, and they have shown that it is possible to maintain stability for hundreds of million years (Bower et al., 2013; Bull et al., 2014; Steinberger & Torsvik, 2012) and their continued existence for billions of years (Mulyukova et al., 2015). But incorporating paleogeographic constraints into mantle convection models (as, e.g., attempted by Flament et al., 2017) requires greatly improved plate tectonic models and numerical codes that incorporate the bridgmanite to post-bridgmanite transition in the lowermost mantle. This important phase transition causes an abrupt viscosity drop of three to four orders of magnitude (Amman et al., 2010; Nakada & Karato, 2012). This weakens slab material, eases and disperses the lateral flow above the core-mantle boundary, and effectively stabilizes and strengthens the LLSVPs against lateral pushing forces (Heyn et al., 2018; Y. Li et al., 2014, 2015).

Testing the stability of the LLSVPs in a robust manner is in fact very challenging. Their stability is observed from LIPs from the Indo-Atlantic realm (Figure 11a) where it is possible to build an absolute mantle reference frame back to 320 Ma (Pangea assembly). The Indo-Atlantic realm includes the bulk of the Earth's continents and oceans that are generally characterized by passive margins (e.g., the Atlantic). Conversely, numerical models for subduction and mantle convection to test their stability are mostly derived from plate models for the Pacific-Panthalassic from where we have no means to develop an absolute plate motion reference frame before the Cretaceous; the Panthalassic (the Earth's subduction "factory") is entirely synthesized before 150 Ma and comprised almost 50% of the Earth's surface.

Earth is a degree-2 planet with two antipodal thermochemical LLSVP piles, TUZO and JASON; modern-type plate tectonics has been operational since at least the Neoproterozoic—and why should Planet Earth be fundamentally different before and after Pangea? There is in fact no evidence for a radical change in the mantle structure associated with Pangea assembly and dispersal—only projected models: Zhong et al. (2007) argued from the outcome of a numerical model that Pangea formed above a major down-welling, and that following continental assembly, a sub-Pangea upwelling later developed as mantle return flow in response to circum-Pangea subduction. In such a model, TUZO should not have existed before Pangea, because convection would have been dominated by a degree-1 mode with only one upwelling above JASON. But during Pangea assembly, the mantle beneath it was littered with cold Rheic slabs, and it is difficult to foresee how that could have turned into an upwelling and the birth of TUZO within a few tens of million years. But perhaps more importantly, Pangea was not a static supercontinent overlying the same part of the mantle for long but drifted systematically northward over the mantle during its existence.

9.2. Paleogeographic Reconstruction of Baltica and Laurentia

Assuming that the TUZO and JASON LLSVPs have remained nearly stationary before Pangea time and that the origin of mantle plumes can be tied to their edges, it is possible to establish a geologically reasonable

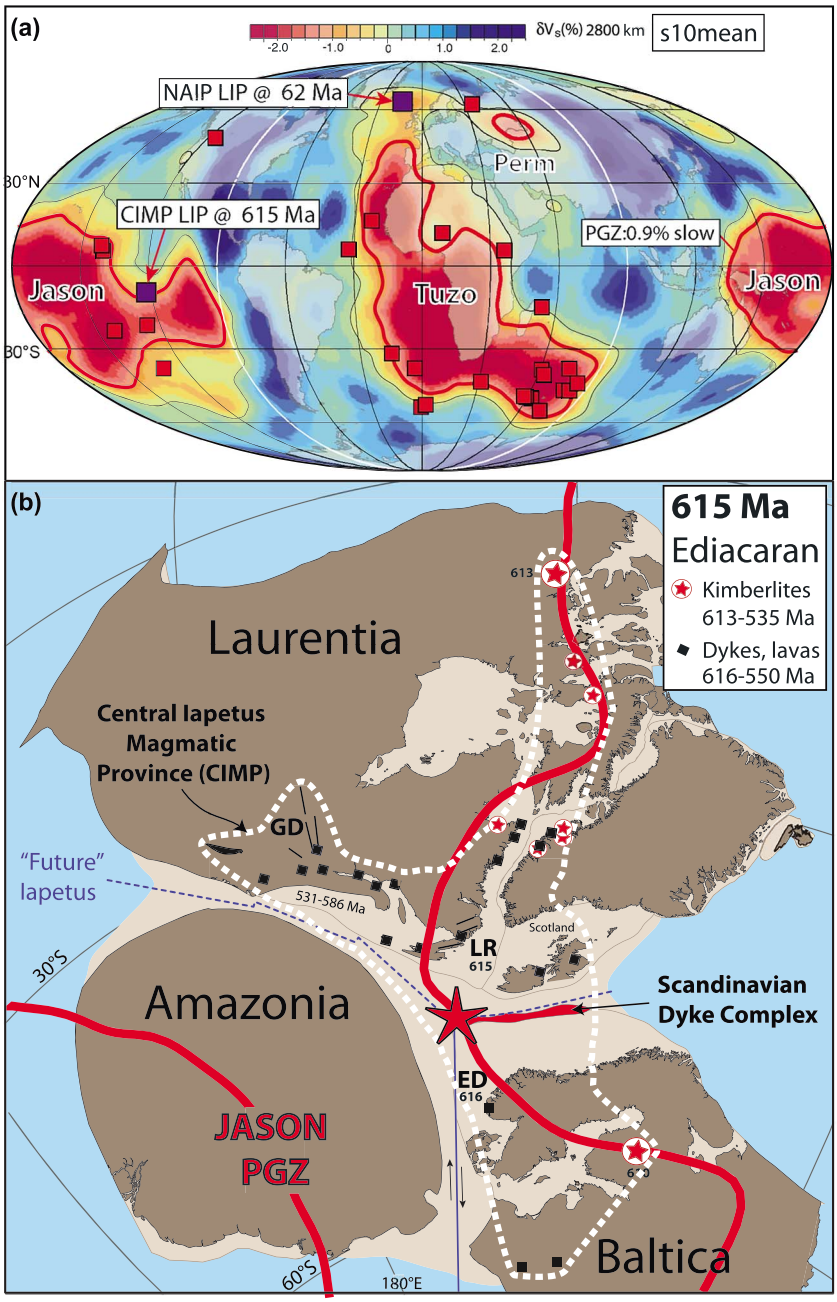

Figure 11. (a) Reconstructed LIPs (15–297 Ma) draped on the s10mean tomography model where the plume generation zone (PGZ) corresponds to the 0.9% slow contour (updated from Doubrovine et al., 2016). Most LIPs overly the PGZs but the Columbia River Basalt is anomalous because it is above a region of faster-than-average anomalies. (b) Paleomagnetic reconstruction of East Rodinia at around 615 Ma using the PGZ reconstruction method calibrated in longitude by LIP related volcanism and kimberlites. The white-dotted line indicates the extent of the Central Iapetus Magmatic Province (CIMP; black squares and lines are dykes as in Figure 1a). Magmatism linked to the CIMP is well preserved in the Caledonian Särv, Seve, and Corrovarre Nappes (central Scandinavia), which are characterized by the spectacular Scandinavian Dyke Complex. The dyke complex was emplaced into continental sediments along the nascent Iapetus margin tentatively located in the paleogeographic reconstruction. We have counterrotated the JASON plume generation zones (thick red line) to account for TPW, so that one can examine how LIP related volcanism and kimberlites directly relate to the PGZs in the paleomagnetic frame. Red star indicate the location of the suggested mantle plume. GD = Grenville Dyke Complex; LR = Long Range Dyke Complex; ED = Egersund Dyke Complex; NAIP = North Atlantic Igneous Province; LIP = Large Igneous Province.

palaeogeographic model for the entire Phanerozoic (Torsvik et al., 2014). In this model the continents are positioned using the latitude from paleomagnetic data, whereas the longitude is defined in such a way that LIPs and kimberlites are positioned above the edges (PGZs) of TUZO and JASON at eruption times. We refer to this procedure as the PGZ reconstruction method, and here we use this method, which also include an iterative TPW correction, to calibrate longitude.

The supercontinent Rodinia, which probably existed in the Neoproterozoic from ca. 1,000 to 600 Ma, has been recognized by most paleogeographers (e.g., Z. X. Li et al., 2008), but the details of its continental makeup are debated (Meert, 2014). Dispersals of both Pangea and Rodinia appear to have been contemporaneous with massive LIP volcanism, with Pangea located above TUZO from its assembly to dispersal, and Rodinia probably located above the antipodal JASON during the Neoproterozoic (e.g., Z. X. Li & Zhong, 2009). Most paleogeographers show Laurentia located next to Baltica and Amazonia in Rodinia and the Late Precambrian breakup of Rodinia led to the opening of the Iapetus Ocean. With reliable paleomagnetic data from the 615 Ma Egersund dykes (Walderhaug et al., 2007) in southwest Norway, we can reconstruct those continents so that LIP-related volcanism and kimberlites plot nearly vertically above the eastern edge of JASON. In this reconstruction—using the PGZ reconstruction method—we moved the continents iteratively in longitude (based on the Egersund paleomagnetic data) and with TPW refinements until we achieved a reasonable fit between (i) an estimated LIP center to explain the formation of the Scandinavian Dyke Complex at a hyperextended margin offshore Baltica (Andersen et al., 2012), (ii) the 616 Ma Egersund dykes (Baltica), (iii) the 615 Ma Long Range dykes (Laurentia), and (iv) contemporaneous kimberlites in Laurentia (613 Ma) and Baltica (610 Ma; Figure 1a). Laurentia, Amazonia, and Baltica are reconstructed to the central-eastern part of JASON, but Figure 11b is a paleomagnetic reconstruction which places Baltica at latitudes between 45° and 75°S, and the JASON PGZ has been counterrotated 70° to account for TPW (see method in Torsvik et al., 2014).

10. Discussion

10.1. Origin of the CIMP

The groups 1 and 2 dyke swarms of CIMP in NE America (Laurentia; see section 2) have compositions very similar to the Scandinavian Dyke Complex (Figures 3 and 6). Many group 1 dykes are intermediate between the compositions of the northern and southern segments in Scandinavia but extend to more enriched compositions similar to the southern segment (Figure 6b; supporting information S11 and S12). The sparsely available data for group 2 also overlap compositionally with those of the southern segment in Scandinavia and extend to more enriched compositions similar to OIB (Figure 6b). Similarly, the transitional to alkali basalt dykes of Egersund in SW Norway plot between enriched MORB and OIB (Bingen & Demaiffe, 1999), and the alkali basalt dykes of the Seiland Igneous Province (Reginiussen et al., 1995) are also close to OIB (Figure 6b). The corollary of this is that similar magma types, all with Th/Yb and Nb/Yb ratios plotting within the oceanic mantle array, were emplaced as dyke complexes in NE Laurentia and SW Baltica, but at variable times. For example, the OIB-like Egersund dykes intruding in situ Proterozoic Baltican basement were an early phase (616 Ma), whereas similar OIB-like magmas of group 2 dykes of Laurentia and of the Seiland Igneous Province were younger (570–550 Ma). Similar magmas of group 1 dykes in Laurentia and the Scandinavian Dyke Complex were emplaced within the same time window from 615 to 590 Ma with most magmatic activity in Baltica between 607 and 595 Ma (Baird et al., 2014; Gee et al., 2016; Svenningsen, 2001); this is probably the most voluminous and intense CIMP event. The compositional variability, the prolonged basaltic magmatism (616–550 Ma), and the eruption over a vast area (>9 million square kilometers, Figure 1) are best explained by melting of multiple, diachronous mantle plume sources upwelling into rifting and thinning continental lithosphere. We surmise that the multiple basalt and kimberlite events of the CIMP (Ernst & Bell, 2010) are best explained by the coincidence of CIMP and a mantle PGZ as depicted in Figure 11. This interpretation corroborates many previous arguments for the involvement of mantle plumes across CIMP (e.g., Andréasson et al., 1998; Bingen & Demaiffe, 1999; Burke & Dewey, 1973; Ernst & Bell, 2010; Hodych & Cox, 2007; Hollocher et al., 2007; Larsen et al., 2018; Puffer, 2002; Seymour & Kumarapeli, 1995).

10.2. The North Atlantic Wilson Cycle: Two LIPs and Two Mantle Plumes?

A comparison of the two LIPs of the North Atlantic Wilson Cycles (NAIP and CIMP) shows that their basaltic magmas are remarkably similar in terms of major and trace element compositions (Figures 3, 6, and 7). Moreover, the structure and magmatic construction (magma-rich margin) of the two continent-ocean transitions have been shown to be very similar offshore Norway today (NAIP) and in the Neoproterozoic (CIMP; Abdelmalak et al., 2015). Similar to our conclusions above, the NAIP has been explained by melting of enriched mantle plume material at elevated ΔT_P (90–210 °C; Brown & Lesher, 2014; Herzberg & Gazel, 2009; Tegner et al., 1998). Moreover, Fitton et al. (1997) showed lateral compositional zoning of NAIP magmas similar to the Scandinavian Dyke Complex (Figure 7a) and explained this as the result of melting of a laterally zoned mantle plume composed in the interior of enriched but heterogeneous mantle surrounded by an outer sheath of more depleted mantle. Another similarity of the two LIPs is the close association with continental breakup. In the Scandinavian Dyke Complex, the Tsäkkok location in northern Sweden (#27, Table 1 and Figure 1) includes pillow lavas (now eclogite) that according to Kullerud et al. (1990) formed within the incipient ocean floor at the thinned edge of Baltica. In NAIP, the first occurrence of oceanic-type low-Ti basalts in the East Greenland volcanic succession was explained as the development of the incipient ocean floor during the main flood basalt event (Tegner et al., 1998). Following Buiter and Torsvik (2014), we therefore propose that the two opening phases of the North Atlantic Wilson Cycles both were associated with LIPs that originated from mantle plumes. The compositional similarity of CIMP and NAIP suggests that the compositions of the two mantle PGZs of JASON and TUZO (Figure 11) may be very similar.

10.3. Can LIPs Be Used as Piercing Points for Plate Reconstructions?

The remarkable correlation of reconstructed LIPs (Figure 11a) and kimberlites suggests long-term stability of TUZO and JASON LLSVPs, and there are therefore strong arguments for their quasi-stability through most of the Earth's history as discussed in section 9.1. Using the PGZ reconstruction method of surface-to-core-mantle boundary correlation to locate continents in longitude and an iterative approach for defining a paleomagnetic reference frame corrected for TPW, we have built an absolute plate reconstruction for East Rodinia in the Ediacaran (615 Ma). In this model, the LIP-related CIMP dyke swarms and lavas and the kimberlites are assumed sourced from the PGZ at the margin of JASON (Figure 11b). Plume-derived magmatism is therefore used as piercing points for absolute mantle-frame plate reconstructions. The PGZ reconstruction method is probably the only way forward to semiquantitatively position continents in longitude before Pangea and has previously been used successfully to reconstruct the 510 Ma Kalkarindji LIP (Western Australia) to the northeastern margin of TUZO (Torsvik et al., 2014). But if TUZO and JASON were highly mobile, or if Earth alternated between degree-2 (two upwellings such as TUZO and JASON and two downwellings as today) and degree-1 modes (e.g., Zhong et al., 2007), then this method is invalidated, and we have no means for calibrating longitude using LIPs and kimberlites as piecing points to derive absolute reconstructions before Pangea.

11. Conclusions

A more than 1,000-km-long magma-rich, pre-Caledonian rifted continental margin of Baltica formed during the Ediacaran. The ~616–590 Ma breakup magmatism following a long period (~200 Ma) of crustal extension and rifting of Rodinia includes prominent dyke complexes in NE America (Laurentia) and NW Europe (Baltica). The Scandinavian Dyke Complex of the magma-rich margin in Baltica is one of several magmatic complexes making up the huge CIMP, a LIP associated with the initiation of the Caledonian Wilson Cycle. Our compilation of new and published geochemical data from the Scandinavian Dyke Complex shows a pronounced lateral variation of ΔNb, La/Sm_N, and Sr isotopes from SW to NE along more than 1,000 km. Geochemical modelling shows this geochemical zoning is best explained by melting related to a broad mantle plume that had elevated potential temperatures (ΔT_P of 75–150 °C based on rare earth elements and ΔT_P of 100–250 °C based on major elements) and was enriched (primitive mantle) in the south and depleted (depleted MORB mantle) in the north. The origin of CIMP appears to have involved several mantle plumes. This is best explained if the segments of Rodinia that broke up in Baltica and Laurentia coincided with a mantle PGZ identified to be located along the margins of one of the two LLSVPs (JASON) in the deepest mantle. We therefore propose the Scandinavian Dyke Complex and other CIMP plumes may be used as piercing points for plate reconstruction, positioning Baltica and Laurentia above the eastern edge of JASON in

the Ediacaran (635–544 Ma). The CIMP formed over a prolonged period between 616 and 550 Ma during the first known, Iapetus, opening stage of the North Atlantic Wilson Cycles. The NAIP was emplaced during the second opening phase, starting at around 62 Ma, and with seafloor spreading initiated at ca. 54 Ma. We therefore conclude that the known opening phases of the North Atlantic Wilson Cycles involved two LIPs and two mantle plumes.

Acknowledgments
Lara O'Dwyer Brown assisted with the compilation of geochemical data and drafting of figures. Svend Joensen assisted with Sr isotope measurements. The data are available as supporting information. This research was funded by the Danish National Research Foundation Niels Bohr Professorship grant 26-123/8 and the Norwegian Research Council CoE-grant 223272 to CEED and to FRINAT Project 250327. The University of Padova, Italy, and a sabbatical stipend from Aarhus University Research Foundation to Tegner provided space and time to write this publication. This work benefitted from constructive and very useful journal reviews and editorial handling of Claudio Faccenna.

References

Abdelmalak, M. M., Andersen, T. B., Planke, S., Faleide, J. I., Corfu, F., Tegner, C., et al. (2015). The ocean-continent transition in the mid-Norwegian margin: Insight from seismic data and an onshore Caledonian field analogue. *Geology*, *43*(11), 1011–1014. https://doi.org/10.1130/G37086.1

Albarède, F. (2003). *Geochemistry. An introduction*. Cambridge: Cambridge University Press. https://doi.org/10.1017/CBO9781139165006

Amman, M. W., Brodholt, J. P., Wookey, J., & Dobson, D. P. (2010). First-principles constraints on diffusion in lower-mantle minerals and a weak D′′ layer. *Nature*, *465*(7297), 462–465. https://doi.org/10.1038/nature09052

Andersen, T. B., Corfu, F., Labrousse, L., & Osmundsen, P.-T. (2012). Evidence for hyperextension along the pre-Caledonian margin of Baltica. *Journal of the Geological Society, London*, *169*(5), 601–612. https://doi.org/10.1144/0016-76492012-011

Andréasson, P. G., Solyom, Z., & Roberts, D. (1979). Petrochemistry and tectonic significance of basic and alkaline-ultrabasic dykes in the Leksdal Nappe, northern Trondheim region, Norway. *Norges Geologiske Undersøkelse*, *348*, 47–71.

Andréasson, P. G., Svenningsen, O. M., & Albrecht, L. (1998). Dawn of Phanerozoic orogeny in the North Atlantic tract; evidence from the Seve-Kalak Superterrane, Scandinavian Caledonides. *Journal of the Geological Society of Sweden GFF*, *120*(2), 159–172. https://doi.org/10.1080/11035899801202159

Baird, G. B., Figg, S. A., & Chamberlain, K. R. (2014). Intrusive age and geochemistry of the Kebne Dyke Complex in the Seve Nappe Complex, Kebnekaise Massif, arctic Sweden Caledonides. *Journal of the Geological Society of Sweden GFF*, *136*(4), 556–570. https://doi.org/10.1080/11035897.2014.924553

Beckholmen, M., & Roberts, D. (1999). Mafic dykes in the Leksdal Nappe at Sørli, Central Norwegian Caledonides: Geochemistry and palaeotectonic implications. *Norges Geologiske Undersøkelse Bulletin*, *435*, 59–67.

Bingen, B., & Demaiffe, D. (1999). Geochemical signature of the Egersund basaltic dyke swarm, SW Norway, in the context of late-Neoproterozoic opening of the Iapetus Ocean. *Norsk Geologisk Tidsskrift*, *79*(2), 69–86. https://doi.org/10.1080/002919699433825

Bingen, B., Demaiffe, D., & Breemen, O. V. (1998). The 616 Ma Old Egersund Basaltic Dike Swarm, Sw Norway, and Late Neoproterozoic Opening of the Iapetus Ocean. *The Journal of Geology*, *106*(5), 565–574. https://doi.org/10.1086/516042

Bower, D. J., Gurnis, M., & Seton, M. (2013). Lower mantle structure from paleogeographically constrained dynamic Earth models. *Geochemistry, Geophysics, Geosystems*, *14*, 44–63. https://doi.org/10.1029/2012GC004267

Brown, E. L., & Lesher, C. E. (2014). North Atlantic magmatism controlled by temperature, mantle composition and buoyancy. *Nature Geoscience*, *7*(11), 820–824. https://doi.org/10.1038/ngeo2264

Brown, E. L., & Lesher, C. E. (2016). REEBOXPRO: A forward model simulating melting of thermally and lithologically variable upwelling mantle. *Geochemistry, Geophysics, Geosystems*, *17*, 3929–3968. https://doi.org/10.1002/2016GC006579

Bryan, S. E., & Ernst, R. E. (2008). Revised definition of large igneous provinces (LIPs). *Earth Science Reviews*, *86*(1-4), 175–202. https://doi.org/10.1016/j.earscirev.2007.08.008

Buiter, S. J. H., & Torsvik, T. H. (2014). A review of Wilson Cycle plate margins: A role for mantle plumes in continental break-up along sutures? *Gondwana Research*, *26*(2), 627–653. https://doi.org/10.1016/j.gr.2014.02.007

Bull, A. L., Domeier, M., & Torsvik, T. H. (2014). The effect of plate motion history on the longevity of deep mantle heterogeneities. *Earth and Planetary Science Letters*, *401*, 172–182. https://doi.org/10.1016/j.epsl.2014.06.008

Burke, K., & Dewey, J. F. (1973). Plume-generated triple junctions: Key indicators in applying plate tectonics to old rocks. *The Journal of Geology*, *81*(4), 406–433. https://doi.org/10.1086/627882

Campbell, I. H. (2007). Testing the plume theory. *Chemical Geology*, *241*(3-4), 153–176. https://doi.org/10.1016/j.chemgeo.2007.01.024

Carmichael, I. S. E. (2004). The activity of silica, water, and the equilibration of intermediate and silicic magmas. *American Mineralogist*, *89*(10), 1438–1446. https://doi.org/10.2138/am-2004-1011

Cawood, P. A., McCausland, P. J. A., & Dunning, G. R. (2001). Opening Iapetus: Constraints from the Laurentian margin in Newfoundland. *Bulletin of the Geological Society of America*, *113*(4), 443–453. https://doi.org/10.1130/0016-7606(2001)113<0443:OICFTL>2.0.CO;2

Chew, D. M., & Van Staal, C. R. (2014). The ocean–continent transition zones along the Appalachian–Caledonian Margin of Laurentia: Examples of large-scale hyperextension during the opening of the Iapetus Ocean. *Geoscience Canada*, *41*(2), 165–185. https://doi.org/10.12789/geocanj.2014.41.040

Coltice, N., Phillips, B. R., Bertrand, H., Ricard, Y., & Rey, P. (2007). Global warming of the mantle at the origin of flood basalts over supercontinents. *Geology*, *35*(5), 391–394. https://doi.org/10.1130/G23240A.1

Corfu, F., Roberts, R. J., Torsvik, T., Ashwal, L. D., & Ramsay, D. M. (2007). Peri-Gondwanan elements in the Caledonian Nappes of Finnmark, Northern Norway: Implications for the paleogeographic framework of the Scandinavian Caledonides. *American Journal of Science*, *307*(2), 434–458. https://doi.org/10.2475/02.2007.05

Davies, D. R., Goes, S., & Sambridge, M. (2015). On the relationship between volcanic hotspot locations, the reconstructed eruption sites of large igneous provinces and deep seismic structure. *Earth and Planetary Science Letters*, *411*, 121–130. https://doi.org/10.1016/j.epsl.2014.11.052

Dempster, T. J., Rogers, G., Tanner, P. W. G., Bluck, B. J., Muir, R. J., Redwood, S. D., et al. (2002). Timing of deposition, orogenesis and glaciation within the Dalradian rocks of Scotland: Constraints from U–Pb zircon ages. *Journal of the Geological Society*, *159*(1), 83–94. https://doi.org/10.1144/0016-764901061

Dewey, J. F., & Burke, K. (1974). Hot spots and continental break-up: Implications for collisional orogeny. *Geology*, *2*(2), 57–60. https://doi.org/10.1130/0091-7613(1974)2<57:HSACBI>2.0.CO;2

Doubrovine, P. V., Steinberger, B., & Torsvik, T. H. (2016). A failure to reject: Testing the correlation between large igneous provinces and deep mantle structures with EDF statistics. *Geochemistry, Geophysics, Geosystems*, *17*, 1130–1163. https://doi.org/10.1002/2015GC006044

Ernst, R. E., & Bell, K. (2010). Large igneous provinces (LIPs) and carbonatites. *Mineralogy and Petrology*, *98*(1-4), 55–76. https://doi.org/10.1007/s00710-009-0074-1

Ernst, R. E., & Buchan, K. L. (2010). Geochemical database of Proterozoic intraplate mafic magmatism in Canada. Geological Survey of Canada, Open File 6016, 1 CD-ROM.

Fettes, D. J., Macdonald, R., Fitton, J. G., Stephenson, D., & Cooper, M. R. (2011). Geochemical evolution of Dalradian metavolcanic rocks: implications for the break-up of the Rodinia supercontinent. *Journal of the Geological Society*, *168*(5), 1133–1146. https://doi.org/10.1144/0016-76492010-161

Fitton, J. G., Saunders, A. D., Norry, M. J., Hardarson, B. S., & Taylor, R. N. (1997). Thermal and chemical structure of the Iceland plume. *Earth and Planetary Science Letters*, *153*(3-4), 197–208. https://doi.org/10.1016/S0012-821X(97)00170-2

Flament, N., Williams, S., Müller, R. D., Gurnis, M., & Bower, D. J. (2017). Origin and evolution of the deep thermochemical structure beneath Eurasia. *Nature Communications*, *8*, 14164. https://doi.org/10.1038/ncomms14164

French, S. W., & Romanowicz, B. (2015). Broad plumes rooted at the base of the Earth's mantle beneath major hotspots. *Nature*, *525*(7567), 95–99. https://doi.org/10.1038/nature14876

Garnero, E. J., Lay, T., & McNamara, A. (2007). Implications of lower mantle structural heterogeneity for existence and nature of whole mantle plumes. *Geological Society of America Special Paper*, *430*, 79–102.

Gee, D. G., Andréasson, P.-G., Li, Y., & Krill, A. (2016). Baltoscandian margin, Sveconorwegian crust lost by subduction during Caledonian collisional orogeny. *Journal of the Geological Society of Sweden GFF*, *139*(1), 36–51. https://doi.org/10.1080/11035897.2016.1200667

Herzberg, C., Asimow, P. D., Arndt, N., Niu, Y., Lesher, C. M., Fitton, J. G., et al. (2007). Temperatures in ambient mantle and plumes: Constraints from basalts, picrites, and komatiites. *Geochemistry, Geophysics, Geosystems*, *8*, Q02006. https://doi.org/10.1029/2006GC001390

Herzberg, C., & Gazel, E. (2009). Petrological evidence for secular cooling in mantle plumes. *Nature*, *458*(7238), 619–622. https://doi.org/10.1038/nature07857

Heyn, B. H., Conrad, C. P., & Trønnes, R. G. (2018). Stabilizing effect of compositional viscosity contrasts on thermochemical piles. *Geophysical Research Letters*, *45*, 7523–7532. https://doi.org/10.1029/2018GL078799

Hill, R. I. (1991). Starting plumes and continental break-up. *Earth and Planetary Science Letters*, *104*(2-4), 398–416. https://doi.org/10.1016/0012-821X(91)90218-7

Hodych, J. P., & Cox, R. A. (2007). Ediacaran U–Pb zircon dates for the Lac Matapédia and Mt. St.-Anselme basalts of the Quebec Appalachians: Support for a long-lived mantle plume during the rifting phase of Iapetus opening. *Canadian Journal of Earth Sciences*, *44*(4), 565–581. https://doi.org/10.1139/e06-112

Holbrook, W. S., Larsen, H. C., Korenaga, J., Dahl-Jensen, T., Reid, I. D., Kelemen, P. B., et al. (2001). Mantle thermal structure and active upwelling during continental breakup in the North Atlantic. *Earth and Planetary Science Letters*, *190*(3-4), 251–266. https://doi.org/10.1016/S0012-821X(01)00392-2

Hollocher, K., Robinson, P., Walsh, E., & Terry, M. P. (2007). The Neoproterozoic Ottfjället dike swarm of the Middle Allochthon, traced geochemically into the Scandian Hinterland, Western Gneiss Region, Norway. *American Journal of Science*, *307*(6), 901–953. https://doi.org/10.2475/06.2007.02

Horni, J. Á., Hopper, J. R., Blischke, A., Geisler, W. H., Stewart, M., McDermott, K., et al. (2017). Regional distribution of volcanism within the North Atlantic Igneous Province. *Geological Society, London, Special Publications*, *447*(1), 105–125. https://doi.org/10.1144/SP447.18

Jakob, J., Alsaif, M., Corfu, F., & Andersen, T. B. (2017). Age and origin of of thin discontinuous gness sheets in the distal domain of the magmapoor hyperextended pre-Caledonian margin of Baltica, Southern Norway. *Journal of the Geological Society of London*, *174*, 541–571.

Jones, T. D., Davies, D. R., Campbell, I. H., Wilson, C. R., & Kramer, S. C. (2016). Do mantle plumes preserve the heterogeneous structure of their deep-mantle source? *Earth and Planetary Science Letters*, *434*, 10–17. https://doi.org/10.1016/j.epsl.2015.11.016

Kamo, S. L., Gower, C. F., & Krogh, T. E. (1989). Birthdate for the lapetus Ocean? A precise U-Pb zircon and baddeleyite age for the Long Range dikes, southeast Labrador. *Geology*, *17*(7), 602–605. https://doi.org/10.1130/0091

Kamo, S. L., Krogh, T. E., & Kumarapeli, P. S. (1995). Age of the Grenville dyke swarm, Ontario–Quebec: Implications for the timing of lapetan rifting. *Canadian Journal of Earth Sciences*, *32*(3), 273–280. https://doi.org/10.1139/e95-022

Kathol, B. (1989). Evolution of the rifted and subducted late Proterozoic to early Paleozoic Baltsoscandian margin in the Torneträsk section, northern Swedish Caledonides. *Stockholm Contributions in Geology*, *42*, 1–85.

Katz, R. F., Spiegelman, M., & Langmuir, C. H. (2003). A new parameterization of hydrous mantle melting. *Geochemistry, Geophysics, Geosystems*, *4*(9), 1073. https://doi.org/10.1029/2002GC000433

Kimura, J. I., Takahashi, T., & Chang, Q. (2013). A new analytical bias correction for in situ Sr isotope analysis of plagioclase crystals using laser-ablation multiple-collector inductively coupled plasma mass spectrometry. *Journal of Analytical Atomic Spectrometry*, *28*(6), 945–957. https://doi.org/10.1039/c3ja30329b

Kirkland, C. L., Daly, J. S., & Whitehouse, M. J. (2007). Provenance and terrane evolution of the Kalak Nappe Complex, Norwegian Caledonides: Implications for Neoproterozoic palaeogeography and tectonics. *Journal of Geology*, *115*(1), 21–41. https://doi.org/10.1086/509247

Kirsch, M., & Svenningsen, O. M. (2016). Root zone of a continental rift: The Neoproterozoic Kebnekaise Intrusive Complex, northern Swedish Caledonides. *Journal of the Geological Society of Sweden GFF*, *138*(1), 31–53. https://doi.org/10.1080/11035897.2015.1055298

Klausen, M. B. (2006). Similar dyke thickness variation across three volcanic rifts in the North Atlantic region: Implications for intrusion mechanisms. *Lithos*, *92*(1-2), 137–153. https://doi.org/10.1016/j.lithos.2006.03.030

Kullerud, K., Stephens, M. B., & Zachrisson, E. (1990). Pillow lavas as protoliths for eclogites: Evidence from a late Precambrian-Cambrian continental margin, Seve Nappes, Scandinavian Caledonides. *Contributions to Mineralogy and Petrology*, *105*(1), 1–10. https://doi.org/10.1007/BF00320962

Larsen, R. B., Grant, T., Sørensen, B. E., Tegner, C., McEnroe, S., Pastore, Z., et al. (2018). Portrait of a giant deep-seated magmatic conduit system: The Seiland Igneous Province. *Lithos*, *296-299*, 600–622. https://doi.org/10.1016/j.lithos.2017.11.013

Lee, C.-T. A., & Chin, E. J. (2014). Calculating melting temperatures and pressures of peridotite protoliths: Implications for the origin of cratonic mantle. *Earth and Planetary Science Letters*, *403*, 273–286. https://doi.org/10.1016/j.epsl.2014.06.048

Lee, C.-T. A., Luffi, P., Plank, T., Dalton, H., & Leeman, W. P. (2009). Constraints on the depths and temperatures of basaltic magma generation on Earth and other terrestrial planets using new thermobarometers for mafic magmas. *Earth and Planetary Science Letters*, *279*(1-2), 20–33. https://doi.org/10.1016/j.epsl.2008.12.020

Li, Y., Deschamps, F., & Tackley, P. J. (2014). Effects of low-viscosity post-perovskite on the stability and structure of primordial reservoirs in the lower mantle. *Geophysical Research Letters*, *41*, 7089–7097. https://doi.org/10.1002/2014GL061362

Li, Y., Deschamps, F., & Tackley, P. J. (2015). Effects of the post-perovskite phase transition properties on the stability and structure of primordial reservoirs in the lower mantle of the Earth. *Earth and Planetary Science Letters*, *432*, 1–12. https://doi.org/10.1016/j.epsl.2015.09.040

Li, Z. X., Bogdanova, S. V., Collins, A. S., Davidson, A., De Waele, B., Ernst, R. E., et al. (2008). Assembly, configuration, and break-up history of Rodinia: A synthesis. *Precambrian Research*, *160*(1-2), 179–210. https://doi.org/10.1016/j.precamres.2007.04.021

Li, Z. X., & Zhong, S. (2009). Supercontinent-superplume coupling, true polar wander and plume mobility: Plate dominance in whole-mantle tectonics. *Physics of the Earth and Planetary Interiors*, *176*(3-4), 143–156. https://doi.org/10.1016/j.pepi.2009.05.004

McDonough, W. F., & Sun, S. S. (1995). The composition of the Earth. *Chemical Geology*, *120*(3-4), 223–253. https://doi.org/10.1016/0009-2541(94)00140-4

Meert, J. G. (2014). Strange attractors, spiritual interlopers and lonely wanderers: The search for pre-Pangæan supercontinents. *Geoscience Frontiers*, *5*(2), 155–166. https://doi.org/10.1016/j.gsf.2013.12.001

Moreira, M., Breddam, K., Curtice, J., & Kurz, M. D. (2001). Solar neon in the Icelandic mantle: New evidence for an undegassed lower mantle. *Earth and Planetary Science Letters*, *185*(1-2), 15–23. https://doi.org/10.1016/S0012-821X(00)00351-4

Morgan, W. J. (1971). Convection plumes in the lower mantle. *Nature*, *230*(5288), 42–43. https://doi.org/10.1038/230042a0

Mulyukova, E., Steinberger, B., Dabrowski, M., & Sobolev, S. V. (2015). Survival of LLSVPs for billions of years in a vigorously convecting mantle: Replenishment and destruction of chemical anomaly. *Journal of Geophysical Research: Solid Earth*, *120*, 3824–3847. https://doi.org/10.1002/2014JB011688

Nakada, M., & Karato, S. I. (2012). Low viscosity of the bottom of the Earth's mantle inferred from the analysis of Chandler wobble and tidal deformation. *Physics of the Earth and Planetary Interiors*, *192-193*, 68–80. https://doi.org/10.1016/j.pepi.2011.10.001

Nystuen, J. P., Andresen, A., Kumpulainen, R. A., & Siedlecka, A. (2008). Neoproterozoic basin evolution in Fennoscandia, East Greenland and Svalbard. *Episodes*, *31*, 35–43.

Pearce, J. A. (2008). Geochemical fingerprinting of oceanic basalts with applications to ophiolite classification and the search for Archean oceanic crust. *Lithos*, *100*(1-4), 14–48. https://doi.org/10.1016/j.lithos.2007.06.016

Pettersson, A. (2003). Jämförande litologisk och geokemisk studie af Sevens amphibolitkompleks i Sylarna och Kebnekaise (in Swedish). Thesis, University of Lund, Sweden.

Plank, T., & Langmuir, C. H. (1992). Effects of the melting regime on the composition of the oceanic crust. *Journal of Geophysical Research*, *97*(B13), 19749–19,770. https://doi.org/10.1029/92JB01769

Puffer, J. H. (2002). A Late Neoproterozoic eastern Laurentian superplume: Location, size, chemical composition, and environmental impact. *American Journal of Science*, *302*(1), 1–27. https://doi.org/10.2475/ajs.302.1.1

Ramos, F. C., Wolff, J. A., & Tollstrup, D. L. (2004). Measuring $^{87}Sr/^{86}Sr$ variations in minerals and groundmass from basalts using LA-MC-ICPMS. *Chemical Geology*, *211*(1–2), 135–158. https://doi.org/10.1016/j.chemgeo.2004.06.025

Reginiussen, H., Ravna, E. J. K., & Berglund, K. (1995). Mafic Dykes from Øksfjord, Seiland Igneous Province, northern Norway: Geochemistry and palaeotectonic significance. *Geological Magazine*, *132*(06), 667–681. https://doi.org/10.1017/S0016756800018902

Roberts, D. (1990). Geochemistry of mafic dykes in the Corrovarre nappe, Troms, North Norway. *Norges Geologiske Undersøkelse Bulletin*, *419*, 45–53.

Roberts, R. J., Corfu, F., Torsvik, T. H., Ashwal, L. D., & Ramsay, D. M. (2006). Short-lived mafic magmatism at 560–570 Ma in the northern Norwegian Caledonides: U–Pb zircon ages from the Seiland Igneous Province. *Geological Magazine*, *143*(06), 887–817. https://doi.org/10.1017/S0016756806002512

Root, D., & Corfu, F. (2012). U–Pb geochronology of two discrete Ordovician high-pressure metamorphic events in the Seve Nappe Complex, Scandinavian Caledonides. *Contributions to Mineralogy and Petrology*, *163*(5), 769–788. https://doi.org/10.1007/s00410-011-0698-0

Rudge, J. F. (2008). Finding peaks in geochemical distributions: A re-examination of the helium-continental crust correlation. *Earth and Planetary Science Letters*, *274*(1-2), 179–188. https://doi.org/10.1016/j.epsl.2008.07.021

Salters, V. J. M., & Stracke, A. (2004). Composition of the depleted mantle. *Geochemistry, Geophysics, Geosystems*, *5*, Q05B07. https://doi.org/10.1029/2003GC000597

Seymour, K. S., & Kumarapeli, P. S. (1995). Geochemistry of the Grenville Dyke Swarm: Role of plume-source mantle in magma genesis. *Contributions to Mineralogy and Petrology*, *120*(1), 29–41. https://doi.org/10.1007/BF00311006

Shumlyanskyy, L., Nosova, A., Billström, K., Söderlund, U., Andréasson, P. G., & Kuzmenkova, O. (2016). The U–Pb zircon and baddeleyite ages of the Neoproterozoic Volyn Large Igneous Province: Implication for the age of the magmatism and the nature of a crustal contaminant. *Journal of the Geological Society of Sweden GFF*, *138*(1), 17–30. https://doi.org/10.1080/11035897.2015.1123289

Solyom, Z., Andréasson, P. G., & Johansson, I. (1979). Geochemistry of amphibolites from Mt. Sylarna, Central Scandinavian Caledonides. *Journal of the Geological Society of Sweden GFF*, *101*(1), 17–25. https://doi.org/10.1080/11035897909452549

Solyom, Z., Andréasson, P. G., & Johansson, I. (1985). Petrochemistry of late Proterozoic rift volcanism in Scandinavia II: The Särv dolerites (SD)—volcanism in the constructive arms of Iapetus. *Lund Publications in Geology*, *35*, 1–44.

Steinberger, B., & Torsvik, T. H. (2012). A geodynamic models of plumes from the margins of large low shear velocity provinces. *Geochemistry, Geophysics, Geosystems*, *13*, Q01W09. https://doi.org/10.1029/2011GC003808

Stølen, L. K. (1994). Derivation of mafic dyke swarms in the Rohkunborri Nappe, Indre Troms, northern Norwegian Caledonides: Geochemical constraints. *Journal of the Geological Society of Sweden GFF*, *116*(3), 121–131. https://doi.org/10.1080/11035899409546173

Sun, S. S., & McDonough, W. F. (1989). Chemical and isotopic systematics of oceanic basalts: Implications for mantle composition and processes. *The Geological Society, London, Special Publications*, *42*(1), 313–345. https://doi.org/10.1144/GSL.SP.1989.042.01.19

Svenningsen, O. M. (1994). Tectonic significance of the meta-evaporitic magnesite and scapolite deposits in the Seve Nappes, Sarek Mts., Swedish Caledonides. *Tectonophysics*, *231*(1-3), 33–44. https://doi.org/10.1016/0040-1951(94)90119-8

Svenningsen, O. M. (2001). Onset of seafloor spreading in the Iapetus Ocean at 608 Ma: Precise age of the Sarek Dyke Swarm, northern Swedish Caledonides. *Precambrian Research*, *110*(1-4), 241–254. https://doi.org/10.1016/s0301-9268(01)00189-9

Tegner, C., Lesher, C. E., Larsen, L. M., & Watt, W. S. (1998). Evidence from the rare-earth-element record of mantle melting for cooling of the Tertiary Iceland plume. *Nature*, *395*(6702), 591–594. https://doi.org/10.1038/26956

Torsvik, T. H., Burke, K., Steinberger, B., Webb, S. J., & Ashwal, L. (2010). Diamonds sampled by plumes from the core-mantle boundary. *Nature*, *466*(7304), 352–355. https://doi.org/10.1038/nature09216

Torsvik, T. H., Smethurst, M., Burke, K., & Steinberger, B. (2006). Large igneous provinces generated from the margins of the large low-velocity provinces in the deep mantle. *Geophysical Journal International*, *167*(3), 1447–1460. https://doi.org/10.1111/j.1365-246X.2006.03158.x

Torsvik, T. H., Steinberger, B., Ashwal, L. D., Doubrovine, P. V., & Trønnes, R. G. (2016). Earth evolution and dynamics—A tribute to Kevin Burke. *Canadian Journal of Earth Sciences*, *53*(11), 1073–1087. https://doi.org/10.1139/cjes-2015-0228

Torsvik, T. H., Van der Voo, R., Doubrovine, P. V., Burke, K., Steinberger, B., Ashwal, L. D., et al. (2014). Deep mantle structure as a reference frame for movements in and on the Earth. *Proceedings of the National Academy of Sciences of the United States of America*, *111*(24), 8735–8740. https://doi.org/10.1073/pnas.1318135111

Volkert, R. A., Feigenson, M. D., Mana, S., & Bolge, L. (2015). Geochemical and Sr–Nd isotopic constraints on the mantle source of Neoproterozoic mafic dikes of the rifted eastern Laurentian margin, north-central Appalachians, USA. *Lithos*, *212-215*, 202–213. https://doi.org/10.1016/j.lithos.2014.11.011

Walderhaug, H. J., Torsvik, T. H., & Halvorsen, E. (2007). The Egersund Dykes (SW Norway): A reliable Early Ediacaran (Vendian) palaeomagnetic pole from Baltica. *Geophysical Journal International*, *168*(3), 935–948. https://doi.org/10.1111/j.1365-246X.2006.03265.x

Wessa, P. (2015). Kernel density estimation (v1.0.12) in Free Statistics Software (v1.2.1). Office for Research Development and Education. Retrieved from http://www.wessa.net/rwasp_density.wasp/

Wilson, A. H., Zeh, A., & Gerdes, A. (2017). In situ Sr isotopes in plagioclase and trace element systematics in the lowest part of the Eastern Bushveld Complex: Dynamic processes in an evolving magma chamber. *Journal of Petrology*, *58*(2), 327–360. https://doi.org/10.1093/petrology/egx018

Wilson, J. T. (1966). Did the Atlantic close and then re-open? *Nature*, *211*(5050), 676–681. https://doi.org/10.1038/211676a0

Zhong, S., Zhang, N., Li, Z.-X., & Roberts, J. H. (2007). Supercontinent cycles, true polar wander, and very long-wavelength mantle convection. *Earth and Planetary Science Letters*, *261*(3-4), 551–564. https://doi.org/10.1016/j.epsl.2007.07.049

Zwaan, K. B., & van Roermund, H. (1990). A rift-related mafic dyke swarm in the Corrovarre Nappe of the Caledonian Middle Allochthon, Troms, North Norway, and its tectonometamorphic evolution. *Norges Geologiske Undersøkelse Bulletin*, *419*, 25–44.